ELSEVIER

Dynamics of Atmospheres and Oceans 27 (1997) 91–134

dynamics of atmospheres and oceans

Atmospheric wave propagation in heterogeneous flow: basic flow controls on tropical–extratropical interaction and equatorial wave modification

Peter J. Webster *, Hai-Ru Chang

Program in Atmospheric and Oceanic Sciences, University of Colorado, Boulder, CO 80309, USA

Received 12 February 1996; revised 14 August 1996; accepted 5 September 1996

Abstract

It is noted that wave propagation in the atmosphere and error propagation in numerical models appear to have preferred geographical loci. However, these paths appear to be more associated with the low frequency background state of the atmosphere than the location of the wave source. Theoretical and numerical models are used to determine the control the basic state has on wave propagation both between the extratropica and the tropics (and vice versa) and within the tropics. Basic states with horizontal and vertical shear as well as longitudinal stretching deformation are studied. It is shown that strong horizontal shear embedded in equatorial easterlies confines modes close to the equator. Weak shear in westerly tropical flow allows modes to project into the extratropics. That is, the degree of equatorial trapping is diminished. Negative stretching deformation acts to trap modes longitudinally so that the western sides of the westerly ducts are accumulation regions. Negative vertical shear inhibits vertical propagation while positive shear enhances propagation.

It is concluded that the basic state is the determining factor in the observed patterns of waves and the locations of errors in numerical weather prediction and climate models. Of particular interest are the westerly duct regions of the eastern Pacific Ocean and the Atlantic Ocean. These regions appear to act as wave attractors for both equatorially trapped modes and extratropical modes propagating towards the equator and also are regions of enhanced vertical propagation. © 1997 Elsevier Science B.V.

* Corresponding author.

PII S0377-0265(97)00003-1

1. Introduction

During the last decade, the ambitions of operational forecast centers has broadened with the extension of forecast range from days to weeks and, more recently, to seasonal-to-interannual time scales. Indeed, experimental prediction shows that there is predictability emanating out of the El Niño-Southern Oscillation (ENSO) phenomena of the tropical Pacific Ocean (Philander, 1990) or the combination of monsoon–ENSO phenomena (e.g. Webster and Yang, 1989, Webster, 1995) extending to a global scale. Such an expansion has gone hand-in-hand with a greater understanding of how the circulation of the planet works and how disparate parts of the system communicate and interact.

Given indications of long-term prediction, international programs have been organized to observe and monitor the ocean–atmosphere climate system and to provide an infrastructure for model development. A major goal of the World Climate Research Programme (WCRP) and the US Global Change Research Program (USGCRP) is the exploration of the predictability of the global climate system on the time scales of days to millenia. Specifically, the WCRP Tropical Ocean–Global Atmosphere (TOGA; WCRP, 1985) program concentrated on monitoring and understanding the behavior of the coupled system on seasonal to interannual periods, assessing its predictability and setting up an operation system to exploit the predictability that was found to exist. TOGA was designed around the paradigm that processes governing interannual variability were centered in the coupled ocean–atmosphere system of the tropics. During the course of the TOGA decade (1985–1994), however, it became obvious that other physical systems, not uniquely located in the tropics, were also of considerable importance. Furthermore, it became apparent that interannual variability was made up of clusters of weather regimes that possesses anomalous locations and frequency of occurrence relative to the anomalous SST (Sea Surface Temperature) distributions. Some clusters may aggregate to provide either the climate anomaly itself or be the remote manifestation of the climate anomaly. These realizations add a temporal and spatial expansion to the predictability issues involved in interannual variability. To facilitate these extensions a new program GOALS (Global Ocean–Atmosphere–Land System) has been developed with the aim of extending predictability to the global domain.

The precept for these programs is that extended-range prediction beyond the average limit of predictability of individual synoptic weather systems will occur either because there are large-scale components of the global system with intrinsically longer predictability time scales than that of individual synoptic weather patterns, or because lower-boundary forcing, which evolves on a slower time scale than that of weather, can impart significant predictability on atmospheric development. On seasonal time scales, the prospect for atmospheric prediction is based on the second premise. The boundary conditions involved include SST, sea-ice extent and temperature, land surface temperature and albedo, soil moisture and snow cover. Variations in lower-boundary conditions result from the coupling of the dynamics of the atmosphere to the dynamics of the underlying surfaces.

An assessment of the potential for seasonal predictability in the extratropics is not as straightforward as that for the large-scale flow in the tropics, essentially because much of the variability in the extratropical atmosphere and oceans is directly associated with internal instability and non-linearity. Considerations similar to those put forward for the tropics suggest, on the one hand, that the extratropical atmosphere may be most predictable in summer when internal variability is weakest. On the other hand a large component of extratropical predictability is of tropical origin, and predictable planetary-scale circulation patterns in the tropics influence extratropical circulations through teleconnections induced by Rossby wave dynamics which are generally largest in the winter season when meridional potential vorticity gradients are strongest (Palmer and Anderson, 1994).

The message to prediction modelling is clear. Instead of just modelling well the dynamics of the extratropics, which may have been sufficient for a forecast of a day or 2 in duration, the phenomenology of the whole globe has now to be taken into account. Such an expansion of domain is the same for extended weather forecasting (week to 10 days) or seasonal to interannual prediction. Simply, the extension of the forecast period means that errors (or processes) occurring in one part of the globe may pollute rapidly forecasts at great distances (influence remote processes) from the source of the error. Thus, a proper parametrization of tropical convection becomes just as important to the prediction of weather over Europe as the observations over Europe itself. For longer term forecasting, a well modelled ocean is just as important as prescribing a consistent ice model over the arctic. As the models are integrated for longer and longer times, forecasts also fall victim to model 'climate drift' where large errors tend to grow (or congregate) in specific regions due principally to model inadequacies (Reynolds et al., 1994). Also, it has become questionable whether an interactive lower boundary can be excluded from the operational models even for weekly forecasts although, clearly, for longer term forecasts an interactive ocean is mandatory. Thus, as the forecast time scales increase, the same problems which plague climate modelling must be tackled and remedied by the operational modeller.

Fig. 1 provides an indication of some of the problems associated with extended range prediction. The analysis comes from the DERF (Dynamic Extended Range Forecasting) data set (Tracton et al., 1989) which consists of 108 individual 30-day forecasts obtained using the US NOAA (National Oceanic and Atmospheric Administration) National Meteorology Center (NMC) operational global model. The panels show the differences between the 108-day average of the initial analyses (i.e. the average of the Day 0 fields of the 30-day forecast) and the 108-day average of the Day 30 forecast field. The fields shown are the 200-mb zonal and meridional wind components (U, Fig. 1(a); V, Fig. 1(b)). In essence, the diagrams indicate the climate drift in the NMC global model. Some major aspects of the model drift are:

1. The magnitude of the difference fields in the tropical zonal wind component (Fig. 1(a)) are large with root-mean-square difference greater than 10 m s^{-1}. In general, the differences are negative suggesting that the model possesses a strong easterly bias when averaged around a latitude circle. On the other hand, the 850-mb winds (not shown) show a westerly bias especially in the regions of the mid-ocean troughs. This bias, together with the upper tropospheric easterly bias, indicates that the equatorial Walker circulation has weakened considerably.

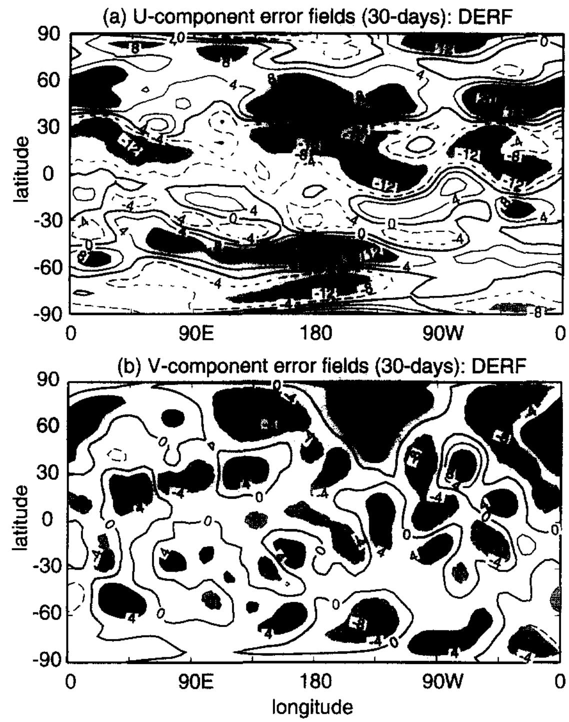

Fig. 1. Climate drift of (a) the 200-mb zonal wind component and (b) the 200-mb meridional wind component in the NMC operational model as obtained from the DERF data set. The DERF data set consisted of 108 consecutive 30-day forecasts. The differences shown here are between the average 30-day forecast and the average initialized data for the same period. (Reynolds, 1993). Dark shading represents positive zonal wind component errors > 8 m s^{-1} (> 4 m s^{-1} for the meridional component). Light shading represents regions of negative component error using the same key.

2. Besides the occurrence of a zonally averaged bias, there is a regional form to the climate drift as well. In particular, the zonal wind field is too easterly by over 15 m s^{-1} in the vicinity of the Pacific and Atlantic mid-ocean troughs. The local enhancement of the easterly bias is sufficiently strong that the upper-tropospheric westerlies in the Pacific and Atlantic Oceans (the ''westerly ducts''; Webster and Holton, 1982) have nearly disappeared.
3. The V difference fields (Fig. 1(b)) show a very strong regionality in the tropics again, the largest differences occur in the vicinity of the mid-ocean troughs. In fact, in the Pacific Ocean the mid-Pacific trough has nearly disappeared and is replaced by a weak ridge.
4. Large errors are evident in the subtropical zonal wind fields (Fig. 1(a)) arising from a polar displacement of the midlatitude jet streams.
5. The distributions shown in Fig. 1 are ambiguous to some extent. As the forecasts were commenced over a 108-day period, the distributions also contain some element of trend as well as model drift and bias.

Although these errors refer specifically to the NMC model used at the time of the DERF forecasts, [1] they are representative of the error fields found in most operational models. For that reason they can be used as a point of general discussion.

The importance of the systematic error depends, of course, on its magnitude relative to the variance of the quantity in question. Webster and Yang (1989) indicate that the variance of U of the equatorial 200-mb zonal wind component is of the order of 8 and 6.5 m s^{-1} in DJF (December, January, February) and JJA (June, July, August), respectively. Variance, in this case, was defined as the power in the transient motions on sub-monthly time scales. Thus, the systematic errors are about a factor of two larger than the observed variance! In view of the global and multi-sphere context of modern forecasts diagrams such as Fig. 1, therefore, present forecasters and other users of a model with a list of difficult questions.

1. What is the cause of the model deviation? For example are the locations of the extratropical jet streams a function of local lower boundary heating parametrization, problems with the way orography is handled in the model or because tropical heating is not treated adequately?
2. Are the errors centers closer to the equator the result of an inappropriate treatment of the interaction of the extratropics and tropics in the region of equatorial westerlies or some type of transmitted error from poorly represented convective or surface heating along the equator?
3. Why do errors appear to aggregate in particular regions, forming 'error centers of action'? For example, why are the U and V difference fields maximized in the eastern tropical Pacific and Atlantic Oceans?
4. How meaningful are long-term integrations or extended weather or climate forecasts made with a model where the systematic error may be larger in certain regions than the local variance?
5. What techniques and means can systematic errors be reduced in the model?

Clearly, systematic errors are not just the problem for operational modellers. General circulation models used in climate simulations and experimentation (which are, in fact, much the same models but integrated for longer periods; Palmer and Webster, 1995) also have errors associated with climate drift. A common strategy in climate modelling is to subtract a perturbed run (the experiment) from a control simulation in the hope that the climate drift is a systematic error and may cancel out. However, implicit in this assumption is that the systematic error behaves linearly and is a function of the model rather than the physical state simulated by the model. Thus, it is in the interests of all modellers to identify the climate drift in a model, understand them and, thus, remove them (Palmer and Webster, 1995).

Besides the study of error propagation in numerical weather prediction models or climate models it is important to understand how one region of the globe connects dynamically with another. Such connections (termed ''teleconnections'' by Bjerknes, 1969) are the vehicles of climatic connections form one part of the planet to another. Anomalies in the tropical heating (e.g. during El Niño) are, perhaps, transmitted to

[1] Updated operational versions are now in use.

higher latitudes by adjustments of these corridors of dynamic connection (Webster, 1981, 1982, Hoskins and Karoly, 1981).

A possible starting point in the analysis of planetary scale geophysical fluid signal communication (either manifested as teleconnections or as an error propagation) is to determine how transients propagate through heterogeneous flow. There are three basic techniques that can be used in this determination:

1. The analysis of climate data: The analysis of real data should show that certain regions are more active than others and that it may be possible to establish causality for this action?
2. Theoretical studies: An examination of the theoretical basis for teleconnections of transient motions and of waves excited in different regions and of the processes which determine the mean (or slower evolving background state) may lead to an understanding of the modification of planetary modes.
3. Systematic experimentation with large scale models: Based upon hypotheses gained from diagnostic studies or theory, experiments can be made with the operational model, preferably in tandem with simpler prototypes or intermediate models.

In the following paragraphs the low frequency variability of the tropics and extratropics will be assessed using a combination of results from observational and theoretical studies. Numerical modelling studies will be restricted to intermediate models used to examine mode aspects in complicated flows that render analytic solutions difficult. Section 2 considers observational evidence of low frequency variability in the tropics and extratropics. In this section the juxtaposition of variance and basic state structure will be established. In Section 3, a theoretical basis is set for understanding of the propagation of errors and teleconnections, in general, in complex basic flows. Conclusions are made in Section 4 together with suggestions for complex model experiments.

2. Observed low frequency variability

The first task is to establish the degree of dependency of transient motions on the variability of the background basic state in the tropics and extratropics. Here the basic state is defined as having a time-scale substantially longer than the transient itself. The structure of the global atmosphere is strongly three dimensional besides possessing a substantial annual and interannual character. That is, at any time, the background flow varies with latitude, longitude and height. This variability raises an interesting question: does the variability of the background flow influence the manner in which communication between remote regions of the globe interact? In other words, is the regionality of the variance noted in Fig. 1 merely the result of ducting by the basic flow inhomogeneities? In the following paragraphs observational evidence will be presented that suggests strong spatial ducting of transients.

2.1. Characteristics of the basic flow at low latitudes

The low latitudes are marked by relatively small zonally averaged wind strength but extremely strong variability in the vertical, zonal and meridional directions. The upper panel of Fig. 2(a) shows the spatial variability of the mean boreal winter 200-mb flow.

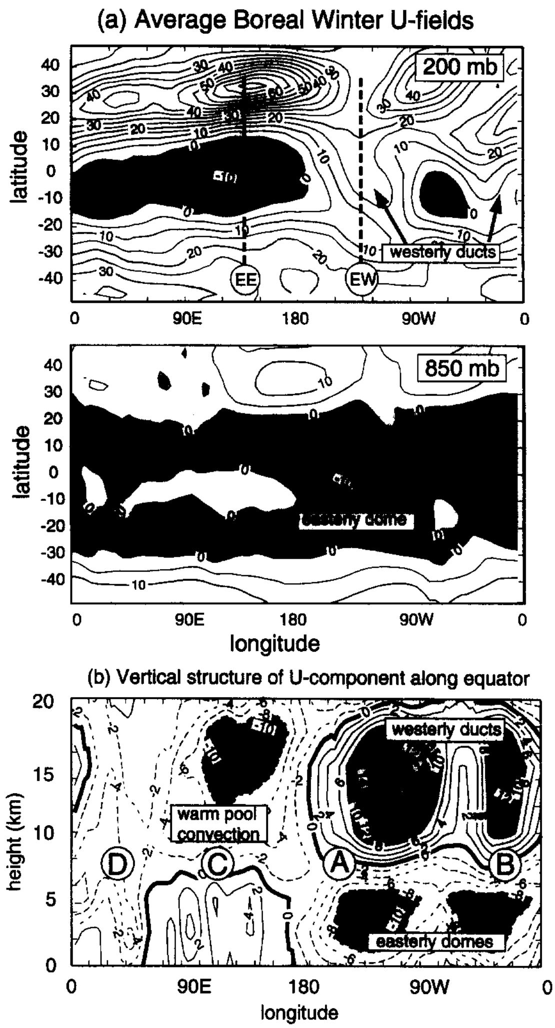

Fig. 2. (a) The long-term average DJF U-field (m s^{-1}) at 200 mb (upper panel) and 850 mb (lower panel). Mean easterlies are shaded. The north–south lines labelled 'EE' and 'EW' indicate regions of very strong shear and weak shear, respectively, for later reference. Note the two westerly ducts (Webster and Holton, 1982) over the eastern Pacific and Atlantic Oceans in the upper troposphere. The strong eastern pacific duct lies over the strongest lower tropospheric easterlies. Tomas and Webster (1994) refer to these easterlies as the 'easterly dome'. (b) Vertical cross-section of $U(x, z)$ along the equator. The dark shading denotes westerly wind > 8 m s^{-1}. Lighter shading indicates easterlies > -8 m s^{-1}. The vertical extent of the westerly ducts and the easterly domes are now very apparent. Note the weak surface westerlies over the eastern Indian Ocean and the Pacific Ocean. The outgoing long-wave radiation sections in Fig. 6(a) indicate that this is a region of maximum deep convection. The lettering indicates regions of differing vertical shear regimes for later reference.

Quite apparent are the regions of weak westerlies that cross the equator in the eastern Pacific Ocean and the Atlantic Ocean. Below the westerly duct in the lower troposphere (lower panel, Fig. 2(a)) are strong easterlies. This region of easterlies is referred to by Tomas and Webster (1994) as the 'easterly dome'. The strong shear in this region and the existence of a critical latitude for the extratropical Rossby waves in the lower troposphere (and not in the upper troposphere) was found to be responsible for the vertical tilting of the equatorially propagating waves as they passed through low latitudes. For later reference, it is worth noting that in the tropical upper troposphere, very strong shear is associated with the easterly regime and weaker shear in the westerly regime. The lines in the upper panel of Fig. 2(a) denoted by 'EE' and 'EW' describe these two regimes, respectively.

Webster and Chang (1988) point out that the horizontal shearing and stretching deformation in the tropics is almost as strong as that which exists in middle latitudes. However, a simple comparison of magnitude is misleading. As the zonally averaged basic winds at low latitudes are weak, the stretching deformation can introduce zeros onto the basic fields. It is these zeros that are critical for accumulation of dispersive waves (Webster and Chang, 1988). The vertical shear is somewhat smaller than in the middle latitudes. In the eastern Pacific Ocean (Fig. 2(b)) the shear is the strongest with and $\partial U/\partial z \approx 30$ m s^{-1} per 10 km. This compares to about double the vertical shear in the East Asia winter jetstream. Even so, the tropical vertical shear will be seen to modify equatorial mode propagation considerably.

In the following paragraphs the impact on equatorial modes of some of the essential elements of the basic state will be considered. In order to facilitate an understanding of the impact of each of the components of the basic flow they will be considered piecemeal. The following components will be considered:

1. Constant basic flows where $U =$ constant. Different values of U will be used in order to determine the impact of the zonally symmetric flow on the characteristics of the basic flow.
2. Zonally symmetric shear flows: $U = U(y)$. Fig. 2(a) showed that there is substantial variability in the strength of the latitudinal shear. How important is the shear in determining the structure of an equatorial mode?
3. Flows with longitudinal stretching deformation: $U = U(x)$. Fig. 2(a) and (b) show that longitudinal stretching deformation changes sign along the equator and reverses sign in the vertical. Is the stretching deformation strong enough to alter the characteristics of the modes?
4. General two-dimensional flows: $U = U(x, y)$. Using shallow water models (linear or non-linear) it is possible to simulate aspects of the observed flow at least at one level or averaged through a slab.
5. Flows with longitudinal stretching deformation and vertical shear: $U = U(x, z)$. The longitudinal stretching deformation occurs in conjunction with vertical shear.

To study the impact of horizontal variations of the basic state, a shallow water system can be used. Such a system may be obtained formally from a full three-dimensional set but with the restriction that there is no basic vertical shear. Thus, consideration of the impact of the vertical variation of the basic flow requires the inclusion of vertical shear (Section 3.3).

2.2. Long-term variability of low latitude flow

Fig. 3 shows the distribution of the correlation coefficient between anomalies in the zonal component of the mean 200-mb velocity (U'; the deviation of U from its mean monthly value) at a reference point (150°W, 0°) relative to U' at all other grid points in the domain. The data set used is the NOAA/NMC mean monthly tropical strip winds. As there is missing wind data in October and November 1972, the data used extend from December 1972 through February 1985, providing a sample of 147 monthly mean fields. There are several major significant correlation areas in the tropics and middle latitudes. These are labelled as A, B, C, D and E. In the tropical region, the most significant positive correlation is located in the neighborhood of the reference point A. A large negative region is located in the area between 330°E and 125°E (B and C). These correlation patterns along the equator imply that the variations of the zonal winds in the central-eastern Pacific are out of phase with winds in the Atlantic and Indian Oceans, a phase difference that varies coherently with time along the equator. Of all reference points along the equator, the correlation patterns are similar with maxima and minima separated by about half of the equatorial circumference. However, the most impressive

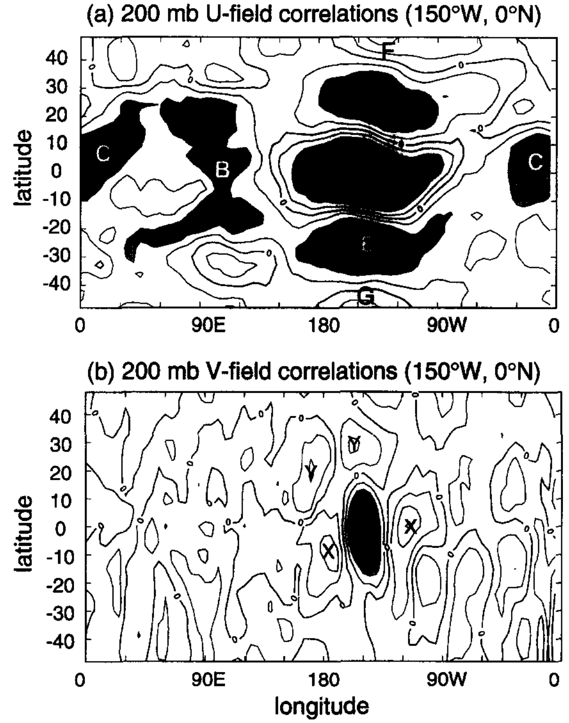

Fig. 3. (a) The correlation fields of the U anomalies at 200 mb relative to the reference point (150°W, 0°N) marked A. The 95% confidence level is at ±3. Areas greater than this level are shaded. Various correlation extrema are marked by letter and discussed in the text. (b) Same as (a) except for the meridional component at 200 mb.

negative correlation occurs between central-eastern Pacific and central-eastern Atlantic, i.e. between the regions 210–240°E and 0–30°E. Correlations for V' show little significance away from the reference point.

In Fig. 3 there are two large statistically significant negative correlation areas away from the equator and immediately poleward of the mid-Pacific westerlies. These are marked by letters D and E and possess central values of -0.64 at 29°S, 140°W, and -0.57 at 24°N, 140°W, respectively. On the poleward sides of the negative correlation areas D and E are two further positive correlation regions (F and G) although their maximum values are somewhat smaller. Thus, in the eastern Pacific Ocean, from the southern hemisphere across the equator to the extratropics of the northern hemisphere, the sign of the correlations alternates. This correlation pattern suggests that there exists wave propagation from the tropics to high latitudes (or reverse) with a lateral modal scale of roughly 40–50° of latitude in the sense described by Hoskins and Karoly (1981) and Webster (1981, 1982).

To study the latitudinal correlation structure in more detail, the reference correlation point is moved along the equator to create meridional correlation strip maps at each latitude. Twelve 30° meridional strips are thus defined between 50°N and 50°S about a reference point on the equator within the strip. Fig. 4(a) shows the distribution of correlations between U' anomalies about a series of reference points and the U' in the

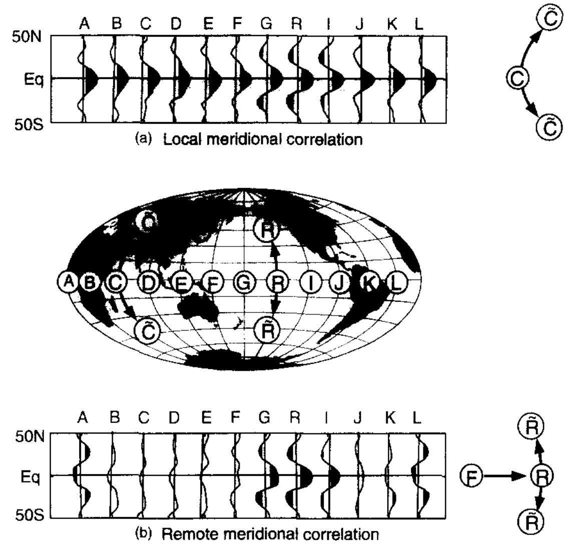

Fig. 4. (a) 'Local' correlation curves indicating the correlation of U averaged in 30° longitude strips as a function of latitude. The curves indicate the correlation of a base point along the equator with the U-field immediately to the north and south. Reference points are located on the equator at 0, 30°E, 60°E, etc. The correlation scheme is summarized in the upper diagram. Shaded parts of the curve donate statistical significance $> 95\%$. (b) Same as (a) except for 'remote' correlation curves indicating the correlation of U at a particular point along the equator (e.g. points A, B, C, ...) with the U-field along the meridional strip centered at 150°W, 0°N (i.e. north and south of R). The remote correlations of most points are stronger than the local correlations of these points shown in (a).

longitudinal strip at all other grid points to the north and south: i.e. the local correlations of U' at (say) point C with those along the local meridian C′–C′. The upper panel describes the scheme. The shaded regions denote statistical significance beyond 95%. Similar patterns appear at all longitudes (i.e. negative correlation between the tropics and high latitudes). An important result is apparent:

- Only in the vicinity of the upper tropospheric westerlies (i.e. between 150°E and 120°W) are the correlations strong and significant away from the equator!

As the correlation value for statistical significance relates to a point correlation, the shaded areas of Fig. 4(a) probably provide an underestimation of the statistical significance.

Fig. 4(b) displays 'remote' tropical-midlatitude correlations. Calculations are based on the location of the strongest local correlations noted in Fig. 4(a). The correlation of U' is plotted at a reference point in a particular longitude belt along the equator with the U' variation along a longitude–latitude strip to the north and south of the mid-Pacific westerly maximum (i.e. in the band between 180°E and 240°E). Alternatively stated, relative to the schematic diagram at the top of the figure, the strips show the variation of the correlation of (say) point C with the 30° averaged correlations along R′–R′ as described in the upper panel. The results of the remote correlations appear rather important:

- Strong communication appears to exist in the strips between 330°E and 30°E and the extra tropics in the reference zone to the north and south of 240°E even though the reference point and reference zone are removed by 180° of longitude! In fact they are stronger than the local correlations north and south of the easterlies shown in Fig. 4(a).

In summary, Fig. 4(a) and (b) indicate that the correlation between the U' along the equator at 0°E is much more strongly coupled with the middle latitudes removed by 180° of longitude away from the correlation point than is related to variability immediately to the north and south.

The remote correlations found in Fig. 4(b) pose an interesting question: Do they mean that the variance generated in the near-equatorial regimes (i.e. generated by mostly convective processes and etc.) communicate with higher latitudes through the westerly ducts? If this is the case, as suggested by the observations, it would be sound evidence for the role the inhomogeneities of the basic state are playing in ducting transients. This will be tested using basic wave theory in Section 3.

2.3. Mean flow, transient energy relationships

Further evidence of the dependency of transients on the configuration of the mean flow is given by Webster and Yang (1989) who compared the spatial characteristics of the kinetic energy of the transients (or the perturbation kinetic energy) and zonal wind fields. The quantities were averaged between 25–35°N and 5°N–5°S for DJF and are shown in Figs. 5 and 6, respectively.

In the extratropics (Fig. 5), the perturbation kinetic energy (PKE) maxima are located between 300 and 200 mb, the height at which the maximum westerlies are found. Great similarity exists between the shapes of the PKE and U except that the maximum PKE

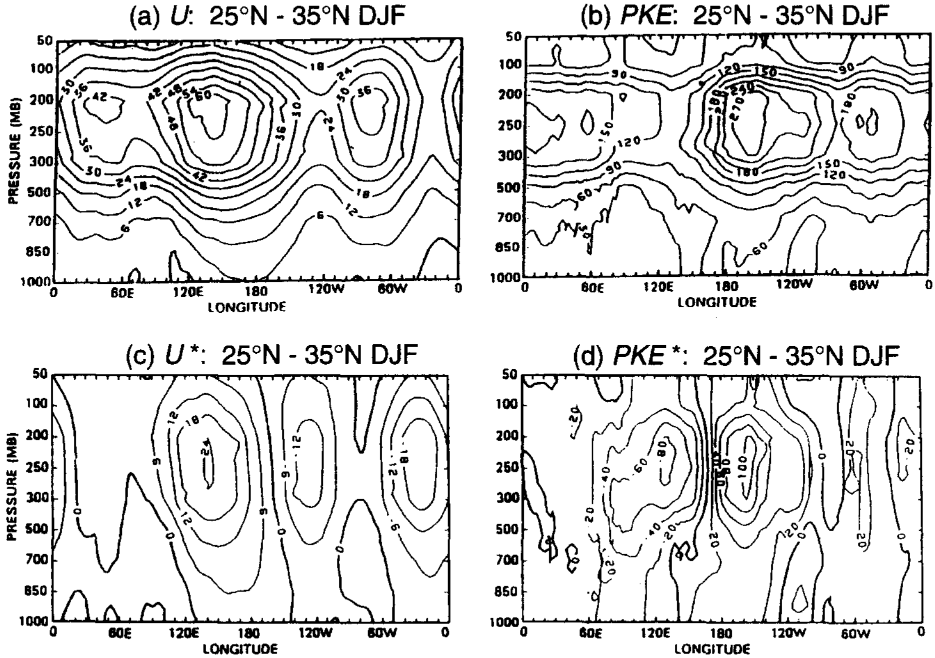

Fig. 5. Height–longitude sections of quantities averaged in the latitude band 25–35°N for DJF. (a) and (b) show the U-field and the PKE and (c) and (d) show the same fields but the zonal average removed (U^* and PKE*). From Webster and Yang (1989).

centers are just downstream of the westerly maxima. Probably this offset corresponds to the location of storm tracks relative to the region of maximum baroclinic instability (Blackmon et al., 1977). These quantities show a minimal tilt with height of both quantities. The structure of the U and PKE fields can be examined further by removing the zonally averaged values at each height. The lower panels of Fig. 5 show U^* and PKE* which have been calculated from quantities with the spatial tonal average removed.

In Fig. 6, the mean OLR (Outgoing Longwave Radiation) along the equator is plotted together with the U and PKE fields. The U-fields show an out-of-phase structure between the lower and upper troposphere in sharp contrast to the near inphase relationship found in the extratropics. Equatorial westerlies extend between 500 and 100 mb in the western hemisphere but are confined to below 700 mb over the Indian Ocean and the western Pacific Ocean. Two westerly maxima exist over the eastern Pacific Ocean and the Atlantic. Easterly winds exist elsewhere and, together with the westerlies, clearly define the Walker circulation along the equator. The removal of the zonal average (lower panels) discloses two cells, the stronger being consistent with the ascent over the warm pool regions of the western Pacific Ocean and with the OLR minimum (top panel). In the upper troposphere, the PKE* maximum occurs in the vicinity of the westerly maxima or in the location of OLR maxima. The PKE* minimum, on the other

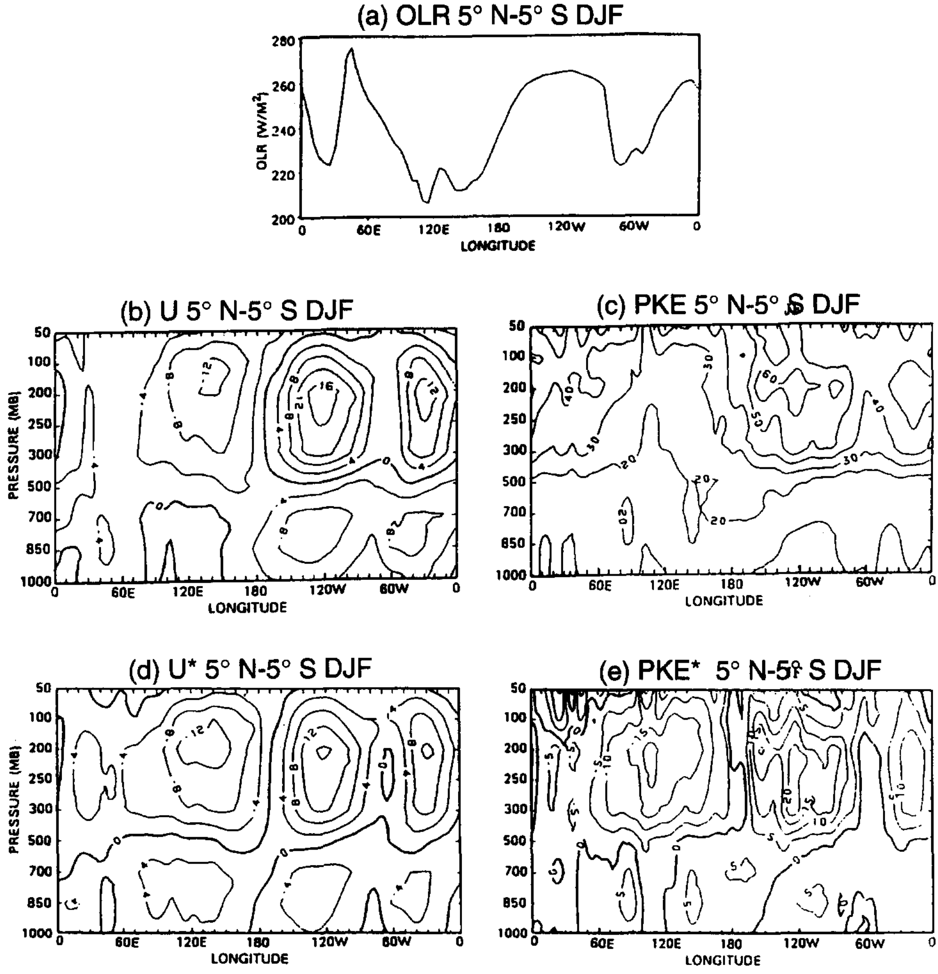

Fig. 6. Same as Fig. 5 except for the latitude band 5°N–5°S. The mean OLR in the band is shown in the upper panel with an inverse scale. Note that regions of maximum convection (minimum OLR) are regions of minimum perturbation kinetic energy. Maximum perturbation kinetic energy lies in the vicinity of maximum westerly winds. From Webster and Yang (1989).

hand, is collocated with the maximum easterly. Thus, in the tropics maximum transient activity occurs where the convection is a minimum as originally noted by Webster and Holton (1982). On the other hand, where there is maximum convective activity there is a minimum in the transient activity.

In the extratropics, the location of the PKE maxima (downstream of the U maxima) suggests that the PKE are produced by hydrodynamically unstable processes. In the tropics, the locations of the PKE may be assumed to be a measure of the activity of the propagating disturbances from the extratropics to the tropics through the westerly duct in the manner of Webster and Holton (1982) and Tomas and Webster (1994) or the

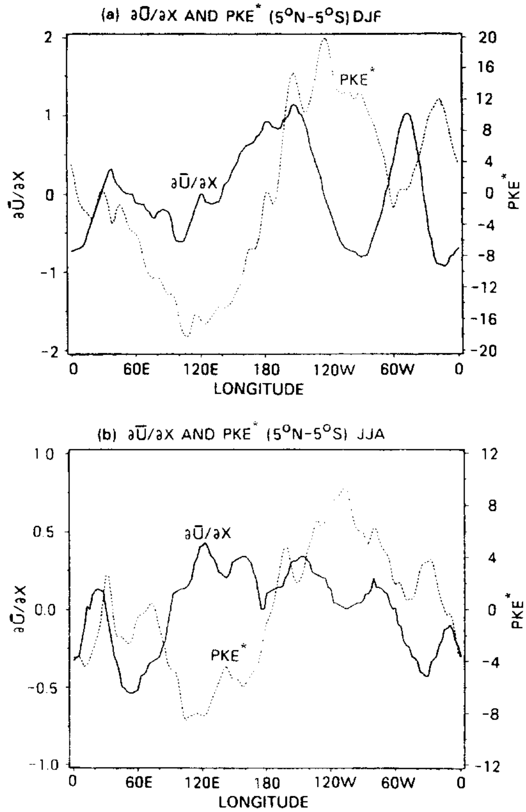

Fig. 7. The longitudinal stretching deformation U_x and PKE* plotted as a function of longitude in the 5°N–5°S band for (a) DJF and (b) JJA. Note change of scale between the two figures. From Webster and Yang (1989).

accumulation of energy as suggested by Webster and Chang (1988) and Chang and Webster (1990, 1995). Alternatively, it could be the combination of both effects which need not be mutually exclusive.

Fig. 7 presents a more detailed view of the relationship of the spatial variability of the basic state and the location of transients. Plots of PKE* and the longitudinal stretching deformation and $\partial U^*/\partial x$ are compared. In winter, the PKE* maxima over the central-eastern Pacific Ocean and the Atlantic Ocean are generally collocated with the maximum negative longitudinal stretching deformation. In summer, the deformation field is much weaker and, although the PKE* is weaker as well, there is still a fairly strong correlation. Wave ray theory (see Section 3.2) states that maximum PKE* should coincide with and $\partial U^*/\partial x = 0$. In Fig. 7 the coincidence is less than perfect. However, besides accumulation there are other factors that are of importance which weaken the relationship slightly. For example, the westerly duct is also a region of intrusion of extratropical waves (Webster and Holton, 1982, Tomas and Webster, 1994). In addition, equatorial waves emanate from the upper tropospheric westerlies towards higher latitudes (Webster and Chang, 1988).

2.4. Role of the basic state in equatorward propagation of extratropical waves

Tomas and Webster (1994) were able to confirm the theoretical prediction of Webster and Holton (1982) that the longitudinal variability of the tropical flow allowed extratropical disturbances to project deeply into the tropical regions. Webster and Holton had noted that considerable transient energy existed in the region of upper tropospheric westerlies in the eastern Pacific Ocean and Atlantic Oceans. They hypothesized that as the Charney (1969) critical latitude did not exist if westerlies spanned the equator between the extratropics that modes should be free to propagate. Numerical experimentation confirmed the hypothesis. Fig. 8 shows wave propagation characteristics on isentropic surfaces roughly representing the 850-mb and 200-mb levels near the equator. In the lower troposphere easterlies (shaded) extend around the equator. In the upper troposphere a broad region of westerly wind exists in the eastern Pacific. Waves propagating towards the equator may be seen to be retarded and distorted as they reach the easterlies in the lower troposphere. At higher levels, where easterlies do not exist, there is clear evidence of interhemispheric propagation.

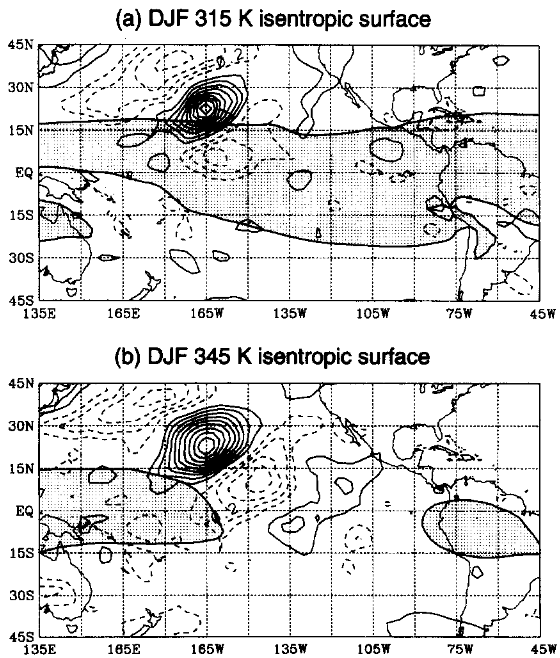

Fig. 8. One point correlation fields formed using the (a) DJF 315 K isentropic potential vorticity (IPV) data (approximately 850 mb near the equator). The base grid point is located at 22.5°N, 165°W. (b) Same as (a) except for the DJF 345 K IPV surface (approximately 200 mb near the equator). From Tomas and Webster (1994).

2.5. Relationships between tropical heating and extratropical jets

The question arises whether it is possible that specific phenomena in one hemisphere can be influenced by specific forcing in the other hemisphere away from the westerly duct. Specifically, do relationships exist between the location and the intensity of the winter hemisphere jet streams and the forcing due to heating in the other, summer, hemisphere?

There are rather important reasons why the variation of the jet stream location and intensity should be investigated. A number of studies (e.g. Blackmon et al., 1977) have shown that the jet streams are source regions of extratropical storms. Thus, variations in the jet stream position and intensity probably impact the loci of weather events, especially in the winter hemisphere. Indeed, it is fairly well known that the storm tracks vary in the extratropics on interannual time scales (e.g. Yang and Webster, 1990). However, the processes which create the jet streams, or define their locations and intensities, together with other mean features of the extratropics, have long been the subject of considerable controversy.

It is whether orographic or thermal forcing determine the location, magnitude and phase of the stationary extratropical waves that has been the source of argument. Whereas there is fairly strong evidence for the dominant role of orography (e.g. Held, 1983, Jacqmin and Lindzen, 1985, Chen and Trenberth, 1988), thermal effects must be important in at least modifying the atmospheric response to orography, Yang and Webster (1990) show clear differences in the location of the extratropical jets and long-wave patterns about their mean seasonal positions during different phases of ENSO.

Fig. 9 shows the simultaneous correlations of the time-mean U-field between 5°N–5°S and 25–35°N (upper panel), between 5°N–5°S and 25–35°S (middle panel), and between 25–25°N and 25–35°S (lower panel). The longitude belts corresponding to the DJF tropical westerlies (the westerly ducts) are marked with heavy lines. Correlations passing the 95% significance level are shaded. In both DJF and JJA, the strongest correlations occur over the central-eastern Pacific Ocean, where tropical westerlies prevail in DJF and relatively weak tropical easterlies appear in JJA. The correlations between the tropics and extratropics are stronger in DJF than in JJA in the northern hemisphere, although they are similar in magnitude in both seasons in the southern hemisphere. A strong negative correlation appears over the central Pacific Ocean in the upper and middle panels; stronger (weaker) equatorial westerlies and weaker (stronger) equatorial easterlies are accompanied by weaker (stronger) extratropical westerlies in both hemispheres. Thus, an in phase change occurs in the extratropical westerlies over the central Pacific Ocean of both hemispheres. Note, too, the strong positive correlations in the lower panel. Although somewhat weaker, negative tropical–extratropical correlations are found over Asia in DJF and over the southern Indian Ocean in JJA, which show the relationship of the extratropical westerly jet streams to the tropical easterlies. In turn, the tropical easterlies are closely associated with the diabatic heating maximum over the eastern Indian Ocean and the western Pacific Ocean, as shown in the following sections. In summary, the maximum cross-equatorial correlation occurs in the region of

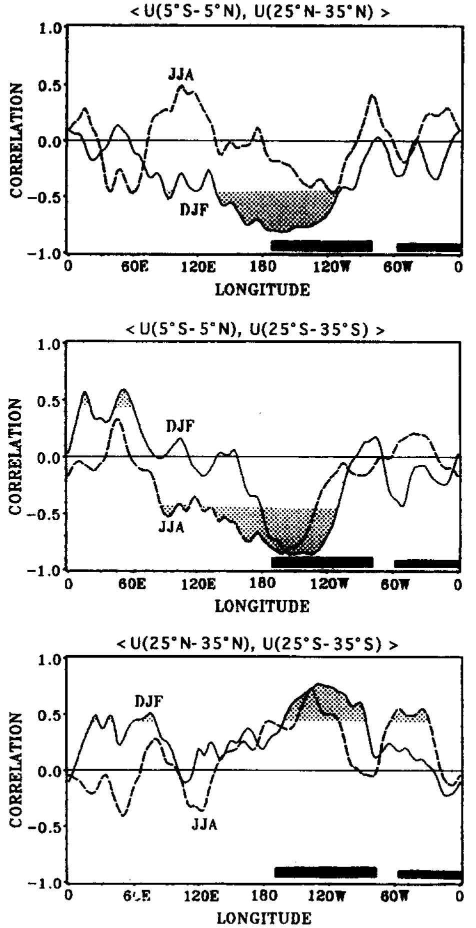

Fig. 9. Simultaneous correlations between U in two different latitude bands for DJF and JJA. Values with $>95\%$ significance are shaded. Thick bars signify the extent of westerlies along equator during DJF. Easterlies prevail during JJA.

the westerly duct. Also, substantial correlations, although relatively weaker, occur between the strength of the equatorial easterlies and the extratropical westerlies.

The variations and correlations that appear in Figs. 4 and 9 are difficult to ascribe just to orography because of the seasonal differences in the jet stream locations and the very large interannual variations. Somehow, the mean zonally averaged flow or an anomalous long-wave pattern must contain the interannual variability produced, perhaps, by heating variation associated with El Niño. This adjusted pattern, in turn, would have to produce an anomalous response with the orographic features in the manner of Chen and Trenberth (1988). Yang and Webster (1990) provide support by showing strong coherence between variations of the heating in the summer hemisphere with changes in the flow in the winter hemisphere. During the El Niño years, the Australian jet stream moves significantly eastward when the subtropical meridional winds (the poleward winds over the southern Indian Ocean and tile eastern Pacific Ocean, and the equatorward winds oven the central Pacific Ocean) shift eastward and decrease in magnitude associated with the eastward migration of the heating in the other hemisphere.

2.6. *Some conclusions from the observational study*

The observational studies discussed in the preceding paragraphs indicate that there is considerable coherent variability between the tropics and the extratropics and between the two hemispheres. Furthermore, it would appear that teleconnection patterns, sympathetic climatic variability and error propagation are controlled by the three-dimensional variability of the background basic state. One point emerges continually. The central Pacific Ocean, in particular, and the Atlantic Ocean, to a lesser extent (or, at least, during El Niño periods), appear as loci for both propagating tropical and extratropical disturbances. As these regions appear to be active across a wide frequency range, it would appear that successful modelling of the global weather or climate should contain a keen representation of these regions. Also, Fig. 1 shows these are the same regions where the models tend to do worst, as evidenced by the maximum systematic error located there.

Perhaps the most interesting conclusion that can be drawn from the observational studies discussed in the preceding paragraphs is that correspondence between the topics and the extra-tropics appears to be very regionalized (Figs. 3 and 6). It is difficult to see evidence for other theories. Sardeshmukh and Hoskins (1988), for example, suggest that non-linear aspects of the divergent flow provide a local source of waves to middle latitudes from the easterlies themselves. If their theory were correct a stronger signal should be expected poleward of the maximum latent heat regions of the tropical Pacific and Indian Ocean warm pools in Figs. 3 and 7. Only very weak local correlations are noted and these are much weaker than the remote correlations which occur from these regions through the westerly ducts.

In the next section it will be shown that the correspondence between centers of transient action and error accumulation should not be surprising. Simple theoretical arguments will show these regions to be dynamical 'attractor' regions for propagating anomalies whether their source is in the tropics or the extratropics. Thus the westerly duct regions appear as 'thoroughfares' for extratropical disturbances and anomalies and, at the same time, locations where wave-energy flux of equatorial disturbances accumulate and from where the equatorial disturbances emanate to the higher latitudes. All of these events arise because of the constraints imposed on wave dynamics by shearing (both horizontal and vertical) and stretching deformations of the basic flow, within which the low-frequency transients reside.

3. Transients in heterogeneous flow

Since the 1960s, through a combination of theoretical and modelling studies, there has been a substantial increase in the understanding of the structure of the tropical atmosphere, its elementary physical nature and its interaction with extratropical regions.

Using a simple primitive equation free-surface barotropic model on an equatorial β-plane, Matsuno (1966) described theoretically the fundamental normal modes of the tropical atmosphere including equatorially trapped eastward propagating Kelvin waves and westward propagating Rossby waves and mixed Rossby-gravity waves. These modes were soon identified in the stratosphere and troposphere by Yanai and Maruyama (1966), Wallace and Kousky (1968) and many others, using diagnostic methods. The identification of equatorially trapped modes was important as the impact of the tropical atmosphere on the general circulation and the interaction between the tropics and midlatitudes had been hinted at by many meteorologists but never formally formulate. A number of recent theoretical works and general circulation model studies (e.g. Simmons et al., 1983, Webster and Chang, 1988, Zhang and Webster, 1989, Chang and Webster, 1990, 1995, Zhang and Geller, 1994 and others) have provided frameworks for evaluating effects of tropical forcing on the extratropical circulation. Simmons et al. (1983) see the evolution of teleconnections patterns resulting from slow instabilities of the two-dimensional global scale basic flow. Webster and Chang (1988) and Zhang and Webster (1989), on the other hand, emphasize the importance of the structure of the slowly varying background basic state on altering the characteristics of transient waves.

3.1. The shallow water system: flows with latitudinal shear

In order to examine the structure of modes relative to complicated basic states a linear, inviscid flow on an equatorial β-plane is defined with a general basic flow $U = U(y)$. The total geopotential field of the system can be expressed as:

$$\phi(x,y,t) = \Phi_0 + \Phi_s(y) + \phi(x,y,t), \quad \frac{\mathrm{d}\Phi_s}{\mathrm{d}y} = -fU \tag{1}$$

where $U = U(y)$, only, and $\Phi = gh$ where h is the depth of the shallow fluid. Furthermore, it is assumed that $\Phi_0 \ggg \Phi_s$.

Following Gill (1982), the equations of motion for the shallow fluid may be written as:

$$\begin{aligned} &u_t + \underline{Uu_x} + \left[vU_y\right] - \mathit{OVERBRACE}\beta yv + \phi_x = 0 \\ &\mathit{OVERBRACE}v_t + \underline{Uv_x} + \beta yu + \phi_y = 0 \\ &\phi_t + \underline{U\phi_x} - \left[\beta yUv\right] + \Phi_0(u_x + v_y) = 0 \end{aligned} \tag{2}$$

A non-zero basic state produces Doppler terms (underlined) and non-Doppler terms (brackets). The usual long-wave approximation (overbrace) is not made (see Gill, 1982). Especially in the case where the flow is allowed to vary as a function of longitude (see Section 3.3) there is the possibility of long waves reducing their horizontal scales substantially, thus rendering the approximation invalid. Furthermore, the long-wave approximation renders dispersive waves non-dispersive and eliminates the mixed Rossby-gravity wave as a class of equatorial modes. In the following development the full primitive set of equations will be used. Little justification is found for the use of the long-wave approximation in almost any circumstance (Chang and Webster, 1995).

The set Eq. (2) can be non-dimensionalized by using time and spatial scales of $\beta^{-1/2}\Phi_0^{-1/4}$ and $\beta^{-1/2}\Phi_0^{1/4}$, respectively. Assuming normal mode solutions proportional to $\exp i(kx-\omega t)$ and making a number of transformations, a governing wave equation in the meridional velocity component can be written as:

$$V_{yy}+\Gamma^2(y)V=0 \tag{3}$$

where $\Gamma^2(y)$ is the refractive index squared.

At the latitude where $\Gamma^2(y)=0$, (i.e. at $y=y_t$ or the turning latitude) the form of the solution chances from wave-like to evanescent. Equatorial trapping requires, thus, that Γ^2 change sign somewhere between the equator and the pole. The refractive index squared is given in non-dimensional form by

$$\begin{aligned}\Gamma^2 = {} & \tilde{\omega}^2-k^2-\frac{k}{\tilde{\omega}}-y^2-OVERBRACE\left(\frac{k}{\tilde{\omega}}U+\frac{U^2}{4}\right)y^2-\frac{1}{2}U\\ & -OVERBRACE\frac{3k^4}{\tilde{\omega}^2-k^2}(U_y)^2-OVERBRACE\frac{k^3}{\tilde{\omega}(\tilde{\omega}^2-k^2)}U_{yy}\\ & +OVERBRACE\left(\frac{1}{2}-\frac{k^3U}{\tilde{\omega}(\tilde{\omega}^2-k^2)}-\frac{2k^2}{\tilde{\omega}^2-k^2}\right)yU_y\end{aligned} \tag{4}$$

where

$$\tilde{\omega}=\omega-kU \tag{5}$$

is the Doppler shifted frequency. The overbraces identify the non-Doppler terms in Γ^2. In general form:

$$\Gamma^2(y)=(a-by-cy^2) \tag{6}$$

where a contains the Doppler terms and b and c the no Doppler terms. In the following section, Eqs. (3)–(6) will be used to explore the impact of the latitudinal shear and the magnitude of the basic state.

3.1.1. Doppler and non-Doppler effects

Zhang and Webster (1989) show that the impact of a non-zero basic state will have no Doppler effects. As the longitudinal scale decreases (k increases) the non-Doppler terms in Eq. (4) increase, especially in westerly basic states. This will be shown to be important in modifying the solutions for weak latitudinal shear westerly basic states that exist in the westerly duct. The impact of the non-Doppler terms is to expand the latitudinal scale. A full discussion is given by Zhang and Webster (1989).

3.1.2. Impact of magnitude and latitudinal shear

The system defined by Eqs. (3) and (4) is now considered for special cases with constant basic zonal wind speeds and flows containing background latitudinal shear.

3.1.2.1. Constant basic flows: $U=U_0$. Following Zhang and Webster (1989), it can be shown that for a constant zonal mean flow, the coefficients of Eq. (6) become:

$$a=\tilde{\omega}^2-k^2-\frac{k}{\tilde{\omega}}-\frac{U}{2},\quad b=o,\quad c=\left(1+\frac{kU}{\tilde{\omega}}+\frac{U^2}{4}\right) \tag{7}$$

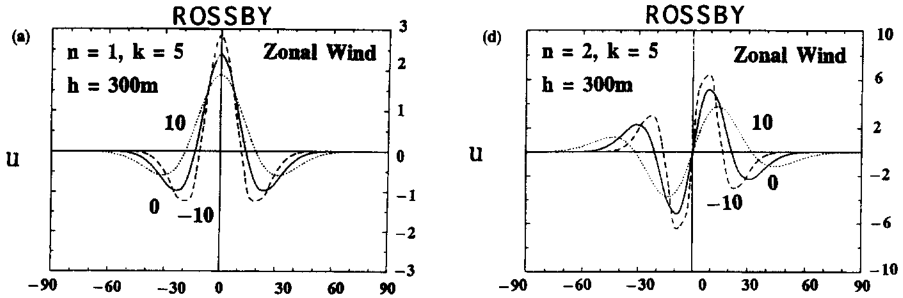

Fig. 10. Structure of the $n = 1$ (upper panel) and the $n = 2$ (lower panel) $k = 5$ Rossby modes as a function of the magnitude and sign of the basic flow. Modes within the westerly basic state are far less trapped than modes in an easterly flow. From Zhang and Webster (1989).

and the refractive index squared reduces to:

$$\Gamma^2(y) = \tilde{\omega} - k^2 - \frac{k}{\tilde{\omega}} - \left(1 + \frac{kU}{\tilde{\omega}}\right) y^2 \tag{8}$$

Here, the terms $U^2/4$ and $U/2$ have been neglected by noting that the non-dimensional $U < -1$ (i.e. dimensional $U \ll \sqrt{gh}$) so that general solutions of Eq. (3) adopt the form

$$\begin{aligned} v(y) &= H_n(K^{1/4} y) \exp\left(-\frac{K^{1/2}}{2} y^2 \right) \\ \tilde{\omega}^2 - k^2 - \frac{k}{\tilde{\omega}} &= (2n+1) K^{1/2} \\ y_t &= \pm (2n+1)^{1/2} R \end{aligned} \tag{9}$$

where $K = (1 + \underline{kU/\tilde{\omega}})$ and R is the modified Rossby radius of deformation defined as $(1 + kU/\hat{\omega})^{-1/4}$. The non-Doppler terms, identified in set Eq. (2), are manifested in the solution as the underlined term in the K definition. Thus, it might be expected that the non-Doppler terms will alter the structure of the solutions and the eigenfrequencies as a function of the horizontal scales. Examination of K (note the underlined term) suggests that the changes to the solutions will not be symmetric for positive and negative values of U.

Fig. 10 shows the structure of the zonal wind of the $n = 1, 2$, $k = 5$ Rossby mode for the different values of the basic state. The modes are much more tightly confined to the equator in the easterlies than in the westerlies. The degree of trapping also decreases as k increases due principally to non-Doppler effect as described above. An examination of Eq. (9) indicates that trapping is decreased at all k but the decrease is maximized for westerly flow.

3.1.2.2. Zonally symmetric shear flows: U = U(y). In order to assess the importance of latitudinal shear, and to see if the effects of a constant basic flow noted in Section 3.1.1, above, would be modified by shear, Zhang and Webster (1989) studied the structure of equatorial modes in a flow $U = U(y)$. The EE and EW configurations of Fig. 2(a) were used.

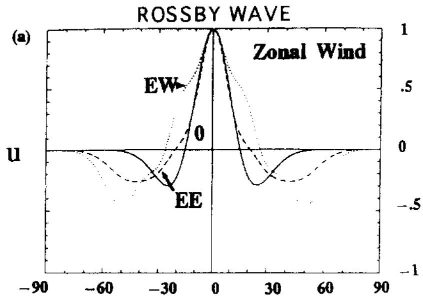

Fig. 11. Distribution of the zonal velocity component of the $n = 1$, $k = 5$ mode in the shear flow similar to the EE and EW basic states from Fig. 2(a). The structure of the mode in a resting atmosphere is shown as the solid line.

With $U = U(y)$ the coefficients a, b and c in Eq. (6) become

$$a = \tilde{\omega}^2 - k^2 - \frac{k}{\tilde{\omega}} - \frac{U}{2} - \frac{3k^4}{\tilde{\omega}^2 - k^2}U_y^2 - \frac{k^3}{\tilde{\omega}(\tilde{\omega}^2 - k^2)}U_{yy}$$
$$b = \left(\frac{1}{2} - \frac{k^3 U}{\tilde{\omega}(\tilde{\omega}^2 - k^2)} - \frac{2k^2}{\tilde{\omega}^2 - k^2}\right)U_y, \quad c = \left(1 + \frac{kU}{\tilde{\omega}} + \frac{U^2}{4}\right) \tag{10}$$

Γ^2 takes on the full form shown in Eq. (4). Following Boyd (1978a,b) and Kasahara (1980), the system can be rendered into a standard eigenvalue problem (Zhang and Webster, 1989).

Fig. 11 shows the structure of the $n = 1$, $k = 5$ Rossby wave zonal wind structure for the two shear profiles EE and EW. Overall, the structure of the modes near the equator is similar for both shear flows. However, away from the equator the amplitude of the mode in the westerly basic shear is much larger. In summary, Zhang and Webster found that in an easterly flow with strong latitudinal shear a mode will be much more tightly trapped to the equator than a mode in westerly flow with weak shear. These two basic state configurations correspond to the upper troposphere of the western Pacific Ocean and the westerly duct regions of the eastern Pacific and central Atlantic Oceans, respectively. Using realistic values for the basic state, Zhang and Webster (1989) showed that an equatorial Rossby mode will be constrained to e-fold within 15° of latitude in easterly flow. In the westerly duct the e-folding distance may increase beyond 30–40°.

3.2. Vertical shear and longitudinal stretching deformation

Fig. 2 showed that there is also considerable variation in the basic state in the longitudinal and vertical directions in the low latitudes as well as with latitude. Instead of a shallow water system, a fully stratified system is needed. Separability is assured by setting $U = 0$ allowing the derivation of both vertical and horizontal group speeds (C_{gx} and C_{gz}) of the modes can be calculated. Using the approximate ray tracing theory of Lighthill (1978) an analytical solution can be obtained in a local frame of reference that moves with the speed of a local flow at each point. Invariants on frequency or wavenumber can be obtained from the kinematic theory of a wave based on the characteristics of the basic flow. With these invariants, the solutions at different locations can be related and used to describe the modification of the wave as it moves through the inhomogeneous flow. The first step is to obtain the local solutions.

3.2.1. Solutions

A motionless basic state is assumed in a frame of reference that moves with a local flow. To accommodate a resting atmosphere, the basic state thermodynamic variables in the local frame must depend on height only. The basic state pressure is assumed to be hydrostatic. On an equatorial β-plane, the linearized perturbational momentum, hydrostatic, mass continuity and thermodynamic equations can be written (after Lindzen, 1967) as:

$$\begin{aligned} &u_t - \beta y v = -\varrho^{-1} p_x \\ &v_t + \beta y u = -\varrho^{-1} p_y \\ &p_z = -\rho g \\ &\rho_t + w\varrho_z + \varrho(u_x + v_y + w_z) = 0 \\ &p_t + wP_z = \gamma\varrho T(\rho_t + w\varrho_z) + (\gamma - 1)\varrho J \end{aligned} \tag{11}$$

in which ϱ, P and T are the density, pressure and temperature of a basic state. u, v and w represent perturbational longitudinal (zonal), latitudinal and vertical velocities. ρ and p are perturbational density and pressure. The constant g represents the acceleration due to gravity, R the universal gas constant, and γ the ratio of specific heats. J is the heating per unit time per unit mass. With the equation of state Eq. (11) forms a complete set. Here z is chosen as the height coordinate to provide the same dimension as x and y.

Following the procedures outlined in Appendix A, horizontal and vertical equations are formed based on the separability assumption:

$$\hat{v} = \sum V_n(z)\Psi_n(y) \tag{12}$$

where $V_n(z)$ and $\Psi_n(y)$ represent vertical and latitudinal structures of $\hat{v}$ separately. h_n represents a separation constant, $H = RT(z)/g$ is the scale height of the basic state, $\epsilon(z) = -\mathrm{d}H/\mathrm{d}z$, and $\kappa = R/C_p$. The horizontal equation is:

$$\Psi_{n_{yy}} + \left(\frac{\omega^2}{gh_n} - k^2 - \frac{k}{\omega}\beta - \frac{\beta^2}{gh_n}y^2\right)\Psi_n = 0 \tag{13}$$

Thus, Eq. (13) is the same as Eq. (6) of Webster and Chang (1988) if it is assumed that $c^2 = gh_n$.

For an isothermal atmosphere, the vertical structure equation Eq. (A3) can be written as:

$$V_{n_{zz}} + \left(\frac{\kappa}{Hh_n} - \frac{1}{4H^2}\right)V_n = -\frac{\kappa^2}{H}S_n \tag{14}$$

following Lindzen (1967). Away from the source area, where $S_n = 0$, Eq. (14) becomes:

$$V_{n_{zz}} + m^2 V_n = 0 \tag{15}$$

where the vertical wavenumber m is defined as:

$$m^2 = \left(\frac{\kappa}{Hh_n} - \frac{1}{4H^2} \right) \approx \frac{\kappa}{Hh_n} \tag{16}$$

Combining Eqs. (13) and (16) gives the dispersion relation for Rossby:

$$\omega = - \frac{\beta k}{\left[k^2 + (2n+1)M \right]} \quad \text{where} \quad M = \frac{\beta}{N}\left(m^2 + 1/4H^2 \right)^{1/2} \tag{17}$$

where $N^2 = g\kappa/H$ and $M = \beta(m^2 + 1/4H^2)^{1/2}/N$ with n representing the latitudinal node number. Here the positive branch of $c^2 = gh_n$ has been chosen.

3.2.2. Horizontal and vertical group speeds

From Eq. (17), the zonal and vertical group velocities are:

$$C_{gx} = \frac{\partial \omega}{\partial k} = \frac{\beta\left(k^2 - (2n+1)M\right)}{\left(k^2 + (2n+1)M\right)^2} \tag{18}$$

and

$$C_{gz} = \frac{\partial \omega}{\partial m} = \frac{(2n+1)\beta^2 k/N^2 M}{\left(k^2 + (2n+1)M\right)^2} \tag{19}$$

Fig. 12(a) shows values of C_{gx} for different values of zonal wavenumbers and equivalent depths. The ordinate is h_n which can be related to vertical wavenumber m through Eq. (16). A large (small) value of h_n corresponds to a small (large) value of m, i.e. a deep (shallow) Rossby wave. For setting $T = 250$ K with $h_n = 100$ meter corresponds to a wave 10.12 km deep, $h_n = 200$ meter to 14.5 km wave, $h_n = 500$ meter to 23.19 km wave, and so on. Thus, for the range of h_n discussed here, the speeds of westward moving Rossby waves decrease monotonically as the values of k increases or as the longitudinal scale decreases. For eastward moving Rossby waves, there is a maximum speed located between $k = 9$ and 14. Variations of h_n (i.e. vertical wavenumber m) also modify the values of C_{gx} especially for long and shallow waves (i.e. small k and h_n). In the range of $3 \leq k \leq 6$ and $300\,\text{meter} \leq 1000$ meter, the value of C_{gx} is almost independent of h_n. For very short waves ($k \geq 11$), C_{gx} depends more greatly on h_n than k. Fig. 12(b) shows the distribution of C_{gz} for different values of k and h_n. For the simple atmosphere used here, the Rossby wave vertical group velocities are always upward. Both k and h_n are very important in determining the values of C_{gz}.

3.2.3. General ray relationships

From kinematic wave theory, it is known that if a background wind field varies in space very gradually, then the relationship between the frequency ω_d in a frame that is fixed in space and the frequency ω in a frame that moves with the same speed as a local

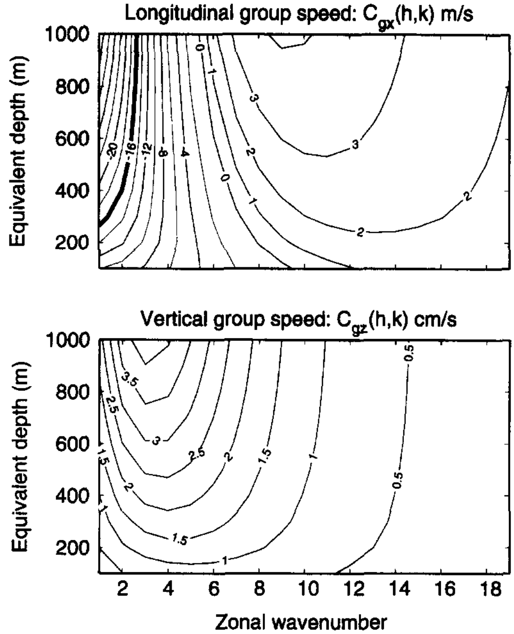

Fig. 12. Distribution of the longitudinal group speed (C_{gx}, m s^{-1}, upper panel) and the vertical group speed (C_{gz}, m s^{-1}, lower panel) as a function of equivalent depth (h_n, m) and zonal wavenumber (k). To the right of the $C_{gx} = 16$ m s^{-1} isotach (darkened), the magnitude of the group speed component may match the magnitude of the westerly winds in the tropical upper troposphere. The longitudinal wavenumber is $n = 1$.

wind can be obtained simply. If the background wind field only has dependencies $U(x, z)$, then the relationship can be written as

$$\omega_d = \omega + Uk \tag{20}$$

where ω is the same as defined by Eq. (17). If a wave is followed with its local group velocity, a ray can be drawn in space. Following Lighthill (1978) and Webster and Chang (1988), the equations that describe the ray are

$$\frac{dx}{dt} = \frac{\partial \omega_d}{\partial k} = U(x,z) + C_{gx} \tag{21}$$

$$\frac{dk}{dt} = -k\frac{\partial U}{\partial x} \tag{22}$$

for the longitudinal direction and

$$\frac{dz}{dt} = \frac{\partial \omega_d}{\partial m} = C_{gz}, \quad \frac{dm}{dt} = -k\frac{\partial U}{\partial z} \tag{23}$$

in the vertical. Here, d/dt represents the derivative following a local group velocity.

3.2.4. Rays in the longitudinal plane

In the upper troposphere the magnitude of the zonal wind varies from about +15 m s^{-1} to about −12 m s^{-1} (Fig. 2). If this velocity range is compared with the zonal group speeds shown in Fig. 12(a) it appears that there is the possibility for modes to possess zero longitudinal Doppler group speeds over a wide scale range. The region to the right of the -16 m s^{-1} group speed isotach (heavy solid line in Fig. 12) defines the modes that potentially possess zero Doppler-shifted group speeds. However, from Eq. (22), a mode may change its scale (and, therefore, its group speed defined in Eq. (18)) if U changes along the ray. Fig. 12 indicates, too, that nearly all modes are candidates for considerable modification of their scale and group speeds.

The impact of slowing the group speed of a mode is to produce a convergence of wave energy flux into a particular region. Whitham (1965) and Bretherton and Garrett (1968) showed that wave action flux is conserved along a ray. In terms of the energy density of a wave, ξ, Webster and Chang (1988) showed that the conservation law can be written for an equatorial Rossby wave as:

$$\frac{\partial \xi}{\partial t} + \left(\bar{U} + \frac{\partial \omega}{\partial k}\right)\frac{\partial \xi}{\partial x} = -\xi \frac{\mathrm{d}U}{\mathrm{d}x} \tag{24}$$

where $\xi = pgh^2$. Thus, in region where the stretching deformation is negative (e.g. to the east of the westerly maximum) there will be a convergence of energy density. Conversely, where $U_x > 0$, there will be divergence of ξ.

Using Eqs. (18), (21) and (22), Webster and Chang (1988) and Chang and Webster (1995) calculated the horizontal Rossby and mixed Rossby-gravity wave propagation in a mean zonal wind field with longitudinal variation. The variation of the basic flow along a ray is not a sufficient condition for wave accumulation (Webster and Chang, 1988). It is also necessary that the magnitude of the basic state and the group speeds of the wave are similar at some point along the ray and that the basic flow changes sign at some location. In the equatorial regions these criteria are met and wave accumulation is possible for most classes and scales of waves except, perhaps, for the Kelvin wave where C_{gx}(Kelvin) $\gg U$ at all points along the equator. It should be noted, however, that there may be exceptions. Tsuda et al. (1994) have found stratospheric Kelvin waves with periods of 20–30 days in Singapore upper air data. For these modes the criterion above would not be satisfied. As the detailed ray path behavior will be strong function of the basic states and different parameter values, a case by case study is required for a thorough elucidation. However, before discussing the individual cases, the results for

Fig. 13. (a) The angular frequency (day^{-1}) plotted as a function of zonal wavenumber, ka and zonal velocity, $\bar{U}$. Positive frequencies are shown as solid lines and negative as dashed lines. Equivalent depth is 500 m. The longitudinal wavenumber is $n = 1$. The letters denote starting or initialization points of the modes in $(k, \bar{U})$ space. For example, point A refers to a $k = 11/a$ mode excited at a longitude where $\bar{U} = 9$ m s^{-1} such that the angular frequency of the mode will be -2.5 day^{-1}. The arrows denote the extent of the wave trajectory in $(k, \bar{U})$ space while the small bars denote trajectory limit if it exists. If there is no horizontal bar, the mode will accumulate and approach zero group speed with increasing wavenumber. (b) Visualization of the Rossby wave characteristics for different basic flows. Heavy dashed arrows denote the path of the wave ray. The horizontal coordinate is longitude. The solid curves represent the speed of the basic state. Four examples are shown: (i) forward accumulation, (ii) propagation (no accumulation), (iii) forward and backward accumulation and (iv) oscillation. The letters correspond to the cases shown in (a). Shaded denotes regions of negative stretching deformation.

Rossby and MR-G waves propagating in relative simple zonally varying basic flows can be interpreted qualitatively by utilizing a straightforward procedure.

Fig. 13(a) (Mixed Russby-Gravity) and Fig. 14(a) show, respectively, plots of the angular frequency (ω) for the Rossby wave and the MR-G wave for different zonal wave numbers k (horizontal axis) and basic flow zonal velocities $\overline{U}$ (vertical axis). The

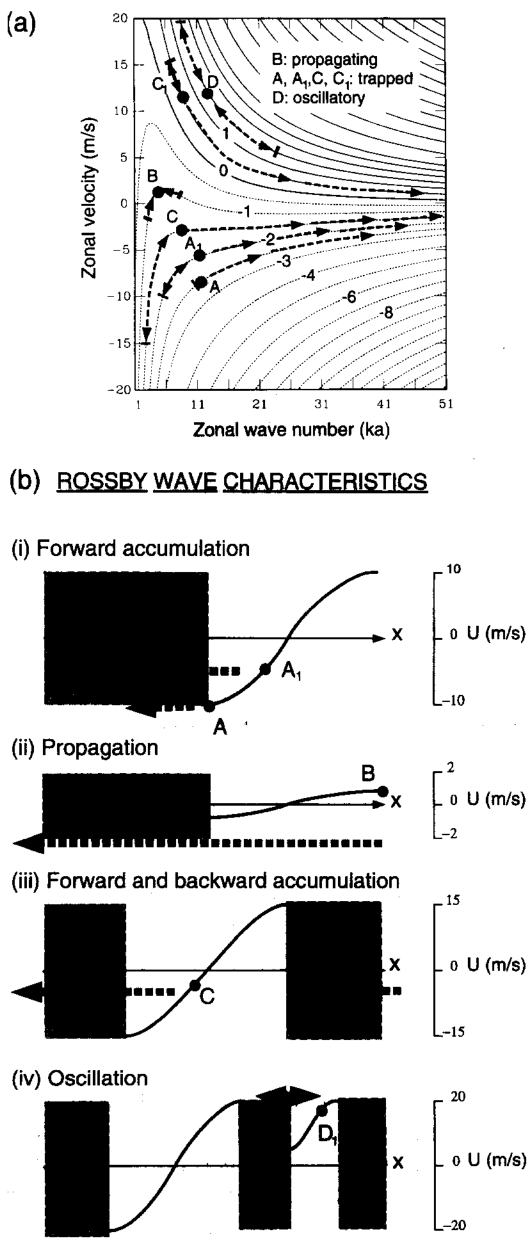

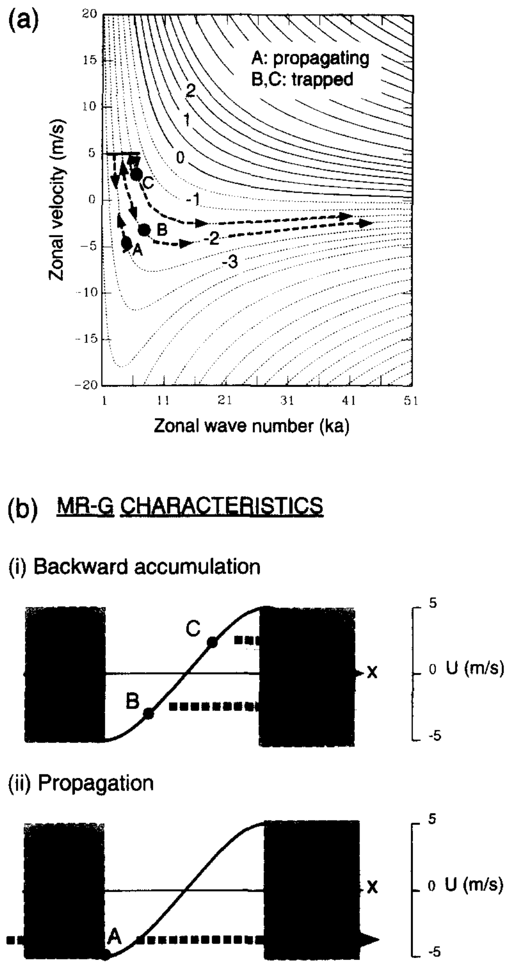

Fig. 14. (a) Same as Fig. 13(a) except for MR-G waves. (b) Same as Fig. 13(b) except for MR-G waves. Two cases are shown: (i) backward accumulation and (ii) propagation.

equivalent depth is set at 500 m representative of the first baroclinic mode observed in the tropical atmosphere. Fig. 13(b) and Fig. 14(b) illustrate the modal trajectories as a function of longitude for the various cases shown in Fig. 13(a) and Fig. 14(a).

3.2.5. Rays in the longitude–height plane

Eq. (23) indicates that if the zonal wind field contains a vertical shear, then m will be changed along a ray. Thus, a reasonable question might be whether or not the transient modes may propagate immediately out of the troposphere before they approach the accumulation regions in the westerly ducts. Also, Eq. (24) shows that m will change along a ray depending on the sign of the vertical shear. From Eq. (16) it can be seen that if m changes then h_n will change, which, from Fig. 12, can alter the horizontal group

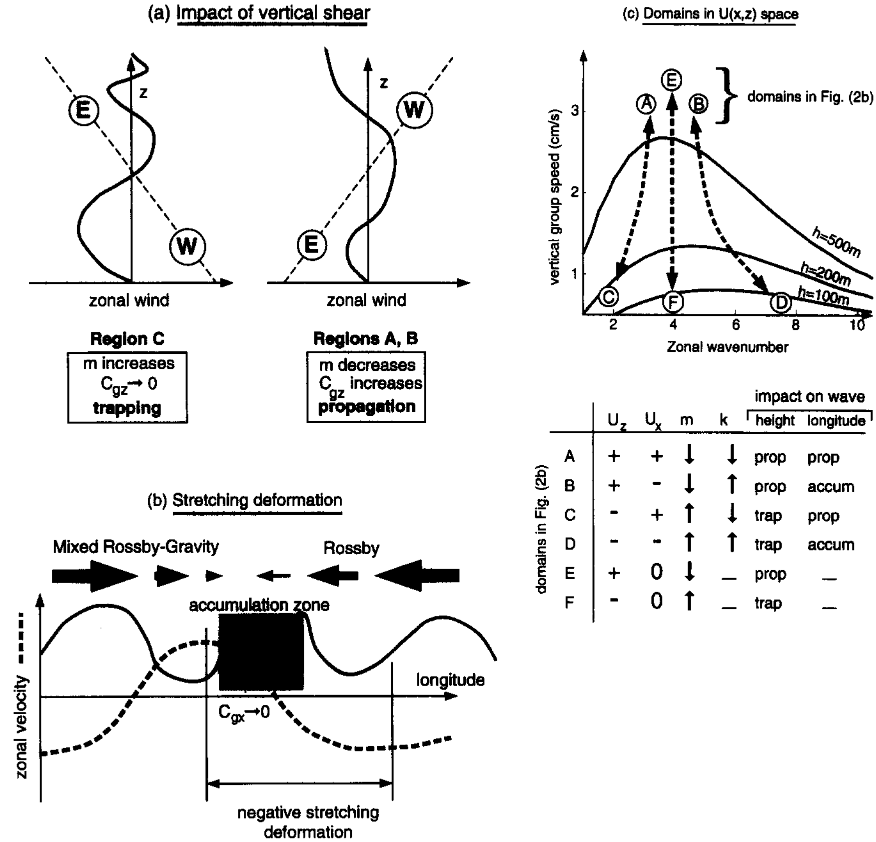

	U_z	U_x	m	k	height	longitude
A	+	+	↓	↓	prop	prop
B	+	-	↓	↑	prop	accum
C	-	+	↑	↓	trap	prop
D	-	-	↑	↑	trap	accum
E	+	0	↓	_	prop	_
F	-	0	↑	_	trap	_

Fig. 15. Schematic diagram describing the vertical propagation of tropical waves (solid curves) in an arbitrary basic state $U(x, z)$ using interpreting Eqs. (21)–(24). (a) For $U_z < 0$, the wavenumber, m, increases (wavelength decreases) and $C_{gz} \to 0$ indicating a vertical trapping of the mode (Region C, Fig. 2(b)). $U_z > 0$, m decreases so that C_{gz} increases and the mode may propagate upwards more rapidly (Regions A and B, Fig. 2(b)). (b) If $U_x < 0$, k increases and $C_{gx} \to 0$ and the mode is longitudinally trapped (accumulation). If $U_x > 0$, k decreases and C_{gx} increases. Arrows show the directions toward accumulation for the Rossby mode (forward accumulation) and the mixed Rossby-gravity mode (backward accumulation). (c) Plot of $C_{gz}(k)$ for various h_n as a function of longitudinal wavenumber. Six regimes are possible. A, B, C and D (see Fig. 2(b)) exist in an arbitrary basic flow $U_{x,z}$. E and F occur when $U_x = 0$. The arrows indicate the 'trajectory' of the rays in (m, k)-space and is summarized in the table for long waves.

velocity C_{gx}. These associations are the reasons why it is necessary to reexamine the results of Webster and Chang (1988) in a $U(x, z)$ basic state.

Fig. 15 presents a schematic version of the influence of a basic state $U(x, z)$ on the modal structure. The inverse relationship between m and h_n from Eq. (16) gives $h_n \propto L_z$, the vertical length scale. That is, the vertical scale goes as the equivalent depth. Then, from Eq. (23), if $U_z < 0$, the vertical scale decreases (i.e. m increases). But if $U_z > 0$, the vertical scale increases (i.e. m decreases). Fig. 15(a) represents Eq. (23) and shows the change of vertical scale for a mode propagating through negative and positive shear regions. Fig. 15(b) describes Eq. (22).

With the relationships between m and U_z established, the interdependency of the vertical and horizontal properties of the modes can be considered. Fig. 15(c) shows the mode trajectories in $(k–m)$ space for arbitrary variations along a ray in a $U(x, z)$ flow. The arrows indicate mode characteristic trajectories for different combinations of stretching deformation and vertical shear referred to in the table in Fig. 15(c). The letters (A, B, C and D labelled in Fig. 2(b)) denote the possible shear-stretching combinations which define unique variations of m and k of a mode propagating through an arbitrary field $U(x, z)$.

Suppose a transient wave is forced in the low level easterlies of the tropics (i.e. a location which would correspond to the convectively active warm pool region of the western Pacific Ocean). Short- and long-wave packets would emerge from the region. The long-wave packet will be confined to the troposphere where $U_z < 0$ (D and C) but will extend rapidly into the stratosphere in the region of positive shear near the mid-ocean troughs (A and B). The short-wave packet, on the other hand, would also be constrained to the troposphere (Region C) during its shorter eastward propagation before arriving at A where it will also rapidly propagate in the vertical in the vicinity of the mid-ocean trough. From Section 3.2 it is recalled that in the same locations (A and B), the modes will also expand in latitude.

Fig. 16 shows rays of Rossby waves in an $x–z$ plane for different values of k and h_n with $n = 1$. The integration period is 15 days which is the time required for a Rossby wave to travel horizontally from an energy source to an accumulation region (Chang and Webster, 1990). Deeper waves (larger value of h_n) will propagate higher than will shorter waves. However, in the tropical atmosphere the quasibiennial oscillation causes great changes to the vertical structure. Integrations (not shown) show that there is substantial inhibition of the vertical propagation of tropical waves during the descending easterly phase.

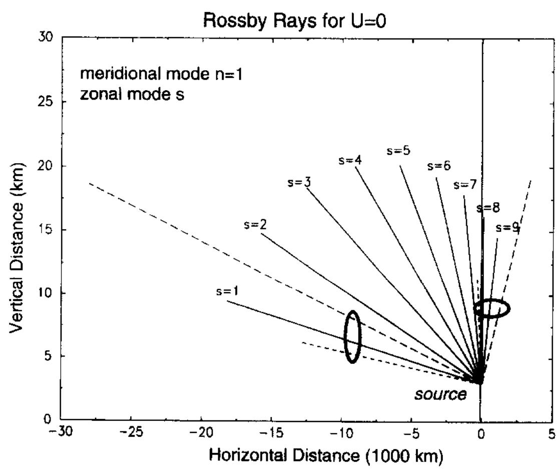

Fig. 16. Rays in the (x, y) plane in a resting atmosphere of the $n = 1$ Rossby mode for different longitudinal wavenumbers. Lines indicate the ray trajectory over a 15-day period. Solid lines show rays for $h_n = 200$ m. Curves for $h_n = 500$ m (dashed) and 100 m are shown for $k = 1$ and 9 as dashed and dotted lines, respectively.

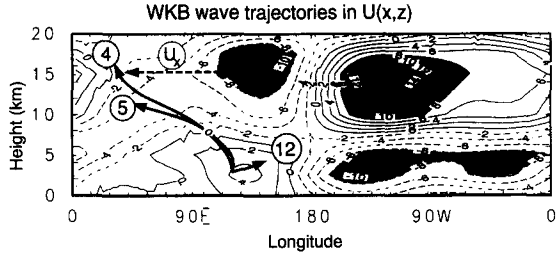

Fig. 17. Smoothed version of the basic state shown in Fig. 2(b) where only the components $k = 0$, 1, 2 and 3 are used. Heavy curves denote the rays of the $k = 4$, 5 and 12 Rossby waves. Heavy dashed curve (marked 'U_x') shows trajectory if there were no vertical shear.

Fig. 17 provides a smoothed version of the mean 1978–85 December zonal wind field in which only Fourier components $k \leq 3/a$ are included where a is the radius of the planet. To apply the ray tracing theory to this more complicated case, it is assumed that the spatial scales of a background wind are much larger than that of the waves that are to be traced. For this basic state, the longest wave must have a zonal wavenumber $k \geq 4/a$ to fulfil WKB (Wentzel-Kramers-Brillouin) requirements. To obtain the proper equivalent depth h_n, Eq. (13) is arranged as:

$$\sqrt{gh_n} = \frac{\alpha\Omega(2n+1)}{S^2\left(\dfrac{2\Omega}{\omega k}+1\right)}\left[-1-\sqrt{1+\left(\frac{\omega}{\Omega}\right)^2\left(\frac{s}{2n+1}\right)^2\left(\frac{2\Omega}{\omega k}+1\right)}\right] \tag{25}$$

where Ω is the angular speed of rotation of the earth. In the equatorial β-plane, Ω is defined as $\beta = 2\Omega/a$. The non-dimensional wavenumber s is defined as $k = sa$. If the initial wavenumber s, angular frequency ω and latitudinal node n of a wave is known, h_n can be obtained from Eq. (23). For a wave with initial $s = 4$, $n = 1$ and $\omega = 2\pi/(10$ days), the value of h_n is 197 m; the corresponding vertical wavelength is approximately 14 km. Solving Eqs. (21)–(24) gives the ray which is superimposed on Fig. 17. The starting point of the tracing is 120°E on the equator and at 3 km height. After a relatively rapid westward propagation, the mode reduces its westward propagation speed and increases its vertical movement. After a 15 days of integration, the wave has reached 31°E and 16 km height. Rays for shorter waves are also plotted. The $s = 5$ mode moves less westward. However, the $s = 12$ wave, representative of the short-wave packet, moves eastward and trapped near the source area.

To separate out the impact of basic wind vertical shear and Rossby wave vertical propagation on the energy accumulation theory from the horizontal effects, the impact of the horizontal stretching deformation separately is considered. Using only Eqs. (21) and (22), and assuming that the 200-mb flow is representative of the zonal flow, the horizontal ray trace can be computed. The temporal variation of the ray is shown as the heavy dashed line in Fig. 17. The farthest the wave propagates is to around 46°E, which is about 15° to the east of the wave that is effected by both the horizontal and vertical variability of the basic state.

To explain the differences between the various components of the background flow, it must realized that along the rays of the two waves different parts of the mean flow are involved. In this way, each wave experiences totally different advecting and stretching regimes although the overall basic wind field is the same. When the vertical variations of the basic state are ignored, the wave experiences a relatively uniform strong negative stretching effect during the entire integration period. For U_x constant, Eq. (22) shows that the k increases exponentially with time. Fig. 13(a) indicates that C_{gx} should decrease exponentially in the early stages of the integration when the wave has a westward group velocity and remain relatively uniform when C_{gx} becomes positive. In the early stages of the integration, the background wind decreases linearly with time and C_{gx} decreases exponentially with time. Toward the end of the integration period, k becomes very large and the C_{gx} becomes positive. The wave still moves westward with a speed decreasing with time, because the background wind still has a negative value that is larger than the value of C_{gx}.

The situation for the wave that propagates in both horizontal and vertical is very different. Given the location of the wave source, the wave first experiences a westerly flow in the lower troposphere. Thus, the wave can only propagate vertically and forward to the east during this time. After the ray moves above the 6-km level, a relatively horizontally uniform easterly wind field appears. During this stage, the wave moves very rapidly to the west because both the background wind and the zonal group velocity C_{gx} have negative values. After the ray reaches 75°E and 11 km height, it experiences a strong negative horizontal stretching and positive vertical shearing effects. From Eqs. (22) and (23), it is known that k will start to increase and m will start to decrease. In fact, the value of C_{gx} will become small and the value of C_{gz} will become large. In addition, the magnitude of the background wind also becomes very small in this region and the wave begins decelerating in the horizontal and accelerating in the vertical. Most of the differences in the ray paths in the $U(x)$ and $U(x, z)$ cases result from the persistently stronger stretching deformation encountered by the wave in the former case.

3.2.6. *Shear flows with deformation:* $U = U(x, y)$

Experiments using a full variability of the basic state (i.e. $U(x, y, z)$) fall into the realm of a general circulation model study. But, as one further intermediate step prior to the use of general circulation models, the impacts of basic states can be considered in which the flow varies in longitude and latitude (i.e. $U(x, y)$) noting the impact of the vertical propagation. That is, where the mode is most vertically trapped in the convective regions of the tropics (i.e. $U_z < 0$), the mode is most equatorially trapped. Only in the regions of positive vertical shear, which coincide with regions of horizontal accumulation, is the vertical mode free to propagate. Thus, the possibility of vertical escape of a mode to the stratosphere before it reaches the region of accumulation is reduced. Additionally, the confinement of the transient wave to the upper troposphere as it moves away from the source region, gives some credence to the use of the upper tropospheric flow as representative of the tropics as used by Webster and Chang (1988) and Chang and Webster (1990, 1995). But, it should be noted, that the total horizontal propagation is different when the vertical propagation is not ignored. With these caveats and remarks in mind, some indication of the impact of the seasonal (or epochal) impact of the basic state on the propagation of transients can be obtained.

Periods of strongest stretching deformation occur during DJF during 'normal' years and the La Niña periods when the westerlies are strongest in the eastern Pacific Ocean. During the El Niño period the westerlies are weak in the Pacific but much stronger in the central Atlantic Ocean. The JJA profile is typical of boreal summers even during the

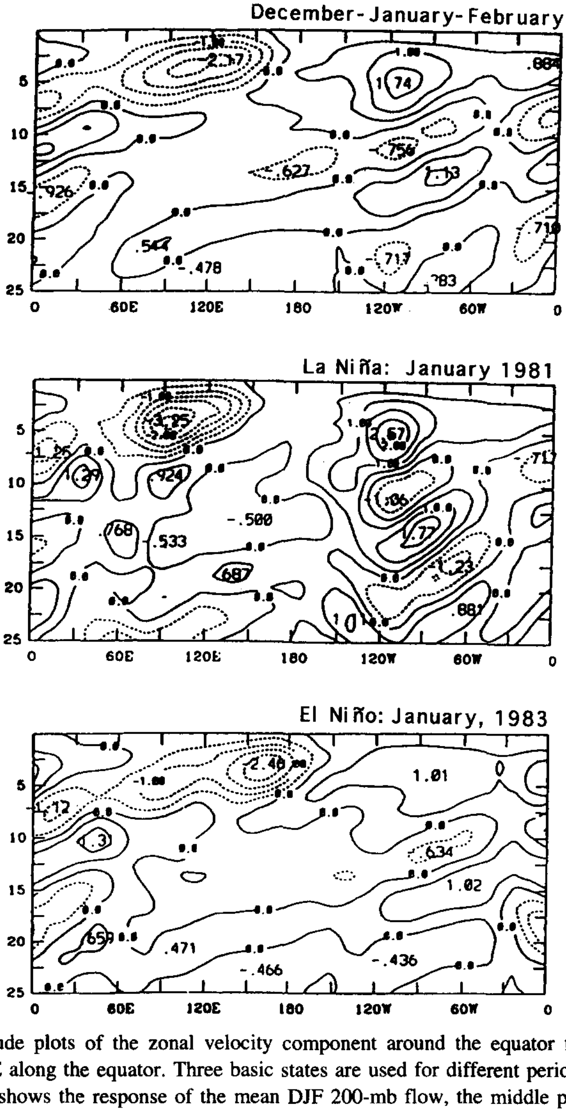

Fig. 18. Time–longitude plots of the zonal velocity component around the equator for 25 days following perturbation near 90°E along the equator. Three basic states are used for different periods of an ENSO cycle. The uppermost panel shows the response of the mean DJF 200-mb flow, the middle panel the response of a typical La Niña flow and the bottom panel the response of an El Niño flow. The model used is a shallow water system with realistic $U(x, y)$ basic fields. During 'normal' times the basic flow is similar to that shown in Fig. 2(a). The westerly duct in the eastern Pacific is strong although not as strong as in a La Niña period. Accumulation can be seen in the eastern Pacific during each of these periods by the almost stationary mode after about 5 days of integration. During El Niño the Atlantic westerly duct is strongest and the Pacific duct diminished. Thus, accumulation occurs preferentially over the Atlantic during this phase of ENSO.

extremes of the Southern Oscillation. At this time of the year the longitudinal gradients of the wind fields are extremely weak.

Fig. 18 shows the corresponding longitude–time sections of the perturbation U-field along the equator for a period of 25 days following episodic forcing in a shallow water fluid of $h_n = 300$ m. The basic states represent the mean DJF for January of the La Niña and El Niño of 1981 and 1983, respectively. The same 2-day e-folding forcing as Webster and Chang (1988) is used. In the DJF and La Niña cases there is very strong accumulation in the Pacific Ocean and weaker accumulation in the Atlantic. During an El Niño the situation is reversed. However, during the summer (JJA) there is virtually no accumulation along the equator at all (not shown).

Fig. 18 suggests that during the year that it may be expected that the location or existence of an accumulation zone in the tropics will vary considerably. Also, during winter there are rather strong influences from the equatorial regions in both mid-ocean trough regions but very little during the summer can be anticipated. During El Niño periods it would seem that the Atlantic would be the principal region of communication. However, during La Niña the region shifts to the Pacific. Fig. 19 summarizes a number of experiments where transients were forced in different, and fairly realistic, basic flows (Chang and Webster, 1995). The arrows indicate the location of the accumulation and emanation (or extension) regions that may be expected during El Niño and La Niña Periods.

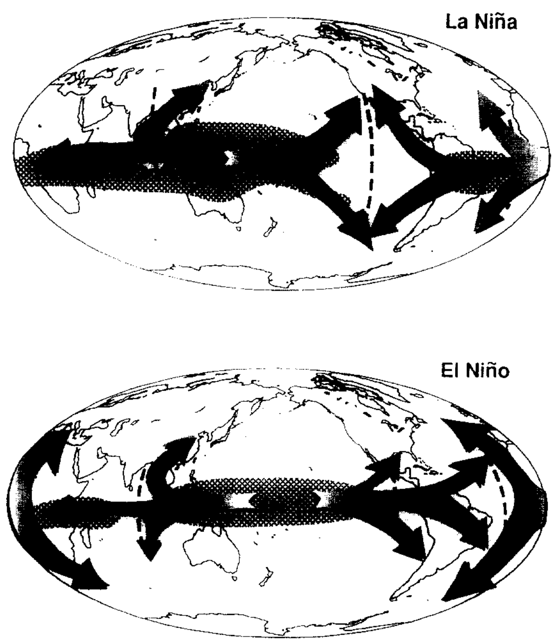

Fig. 19. Schematic diagram showing the paths of equatorial transients that may be expected during extremes of the SOI. The hatched region denotes easterlies in the basic state. During an El Niño, the major communication between the tropics and the extratropics would be in the Atlantic Ocean compared with the Pacific during La Niña. After Chang and Webster (1995).

3.2.7. *General flows:* $U(x, v, z)$

At least two studies of the accumulation/emanation phenomena have been made using full global multilevel models. The first, which used the NOAA/NMC operational model, is reported in O'Lenic et al. (1985) and Frederiksen and Webster (1988). In a number of experiments the model was perturbed in different regions by the introduction of errors into specific regions of the tropics. These initial experiments were an attempt to ascertain the importance of 'uncertainty' in the initial state in introducing errors into a forecast. As it is very difficult to determine the errors involved in a particular initial data set, the 'uncertainty' was defined as the difference between two realizations of the 'same' data set by two different operational centers. Thus experiments were run using the NMC initial data but with ECMWF (European Center for Medium-range Weather Forecast) data planted in different regions. The results were then compared to a standard run. The experiments showed that the response either in the tropics or extratropics was relatively independent of where the data transplant was made. The maximum tropical perturbation was always in the regions of upper tropospheric westerlies along the equator (i.e. the Atlantic and the Pacific) and the maximum extratropical perturbation occurred over Europe. The results were interpreted as evidence that the transient modes generated in the error source regions (i.e. where the ECMWF data was inserted) were accumulating and emanating from the mid-ocean trough regions. Gelaro (1990), using the NEPRF (Naval Environmental Prediction Research Facility) model found similar indications of regional activity.

3.3. *Interaction reciprocity between the tropics and the extratropics*

In the preceding paragraphs, it has been emphasized that the modification of transient equatorial modes in realistic basic flows and the manner in which these modes, through their modification, extend into and influence higher latitudes. Theoretical arguments have clarified observations which indicate that the influence towards the extratropics would pass through the mid-Pacific and Atlantic Ocean regions principally because they are regions of upper-tropospheric westerlies. However, an earlier study by Webster and Holton (1982) indicated that extratropical disturbances also enter the tropics, or propagate through to the other hemisphere, in these same regions. They argued that low frequency modes would not encounter a critical latitude when westerlies extend from hemisphere to hemisphere may be inferred from Fig. 10. The results of their numerical experiments are very similar to the diagnostics produced by Tomas and Webster (1994) shown in Fig. 8.

It seems reasonable to use the results presented in this paper to reinterpret the hypothesis of Webster and Holton. Here it has been shown that, as an equatorial mode moves into the equatorial westerlies, it will extend laterally towards the poles. That is, the mode becomes less trapped. Thus, a complete set of modes would include those which would have turning latitudes which extend well into the higher latitudes. If it is imagined that some form of transient forcing develops in the north Pacific Ocean to the north of the equatorial westerlies, then, from a formalistic perspective, the forcing could project onto an extended equatorial mode. In this manner, extratropical transients could force equatorially trapped modes. On the other hand, forcing outside the turning latitudes of the extended equatorial modes would not project onto an equatorial mode and would not influence the tropics.

4. Conclusions

A combination of observational and theoretical studies have examined the role of the slowly varying background state in modifying the behavior of transients. These transients, modes that exist on time scales less than the seasonal, are responsible for the transmission of signals from one part of the globe to another.

In the following paragraphs the results are assimilated and conclusions drawn regarding climate teleconnections, error propagations and modelling.

4.1. Observational and diagnostic studies

Using data it was possible to define the mean structure of the background state of the tropics. Subsequent investigation showed that a knowledge of the mean structure of the atmosphere was critical to allow an understanding of the motion and modification of transients. The following points summarize the pertinent findings.

A strong modulation of the tropical atmosphere on annual and interannual time scales was found. The annual modulation appears to be very similar to that of the ENSO cycle although on time scales about one quarter the length. The mean summer state is quite similar to that during the warm phase of ENSO. In both cases the zonally averaged easterlies are stronger, longitudinal stretching deformation is weaker throughout the entire tropics and the westerly duct in the Pacific ocean almost disappears. On the other hand, during winter, and during the cold phase of ENSO, the mean easterlies are weaker, the stretching deformation is stronger and the westerly duct in the Pacific Ocean attains mean monthly speeds near 20 m s^{-1}.

There is considerable coherence between the long-term variations from one part of the tropics to other parts of the tropics. At the same time there is a strong correlation between the tropics and higher latitudes but this correlation is a maximum in specific longitudinal belts which coincide with the regions of equatorial upper-tropospheric westerlies, or, the mid-ocean troughs. Furthermore, the correlations between the tropics and the extratropics in the vicinity of the mid-ocean troughs are tied strongly to the phase of the ENSO cycle.

Changes in the low-frequency back ground flow were not restricted to the tropics. Strong relationships were also found between the variations of the summer hemisphere convection and the strength and location of the winter hemisphere jet streams.

The extratropical westerly jet streams in the winter hemisphere are poleward of the tropical OLR minima in the summer hemisphere. During DJF, the jets over Asia, North America and Europe are associated in longitude with the heating maxima over Indonesia, South America and South Africa, respectively. During JJA, the jet maxima over Australia, South America and South Africa are associated with the heating maxima over the Asian monsoon regions, North America and North Africa, respectively. These results, presented in Yang and Webster (1990), corroborate the earlier findings of

Krishnamurti (1979). In addition, the location of the major southern hemisphere winter jet stream is keenly associated with the location of the cross-equatorial flow from the convective heating regions of East Asia. Furthermore, the annual changes of the intensity of the extratropical westerly jets in the winter hemisphere are in phase with those of the three maximum heating centers in the tropics in the summer hemisphere.

When the heating is strong in the Australian monsoon regions during DJF, the subtropical poleward wind becomes stronger. This leads to a stronger extratropical westerly jet stream over Asia at a location to the west and stronger equatorward wind over the northern central Pacific Ocean. As the stronger heating in those regions increases the longitudinal heating gradient between the western and central Pacific Ocean, the equatorial westerlies become stronger. During DJF, both the easterlies over the Indonesian regions and the westerlies over the central Pacific Ocean intensify when the heating is stronger over Indonesia. When the maximum heating center moves eastward and the heating locally weakens in the Australian monsoon regions, the poleward wind becomes weaker and shifts eastward. This may lead to an upstream weakening of the jet when the tropical heating weakens significantly. As the eastward migration of heating increases the latitudinal heating gradient in the central Pacific Ocean, a significant downstream strengthening of the jet may be found. At the same time, the warming of the central Pacific Ocean is accompanied by a weakening equatorward wind in those longitudes over the North Pacific. The Australian monsoon heating and Asian jet stream association is related to the ENSO cycle, especially the changes in the downstream portion of the jet, and is shown in Fig. 9(b).

When the heating is stronger in the Asian monsoon regions (especially East Asia) in JJA, the extratropical westerly jet stream over Australia and the subtropical meridional winds over the southern Indian Ocean and the central Pacific Ocean become stronger. When the maximum heating moves eastward and the heating weakens in the Asian monsoon regions, the meridional winds become weaker and shifts eastward. This leads to a remarkable upstream weakening and a significant downstream strengthening of the Australian jet stream together with a weakening equatorward wind over the southern central Pacific Ocean. The Asian monsoon heating and Australian jet stream association, stronger than the association between the Australian monsoon heating and the Asian jet in DJF, and more closely related to the ENSO cycle, is shown in Fig. 9(c).

Specific relationships were found between transients and the mean flow defined in the previous paragraph. Distinct maxima and minima of PKE exist in the tropics which correlate, respectively, with upper tropospheric westerlies and easterlies (Arkin and Webster, 1985, Webster and Yang, 1989). The importance of these correlations is that the tropical mid-ocean trough region is very active with relatively high frequency transients. At the same time, these are the regions of maximum variability in the lower frequency mean flow. The maxima in PKE were found to be in the regions of negative stretching deformation. That is, to the east of the westerly maxima which is consistent with the expectations of Webster and Chang (1988). This association is clearer when the zonal average of the PKE is removed and PKE* examined.

Finally, it was noted that the mid-ocean trough regions are also corridors for the interaction of higher latitude and the tropics. The results of Tomas and Webster (1994) were used to show that propagation by extratropical waves could occur well into the tropics or even into the adjacent hemisphere in the region of the mid-ocean troughs or in the vicinity of the westerly ducts. As the westerly ducts possess a strong annual and interannual variability in their location and strength, the degree of penetration of extratropical waves should also vary. In fact, Prinn et al. (1992) has used the variations of transport through the westerly duct to explain the annual and interannual variability of methyl chloroform in the southern hemisphere.

4.2. Dynamical studies

The relationship between the transients and the character of the background flow motivated a detailed study of the impact of realistic basic flows on transient wave modes. The aim of the examination was to see if there was a dynamical basis for the congregation of transient activity in certain regions of the tropics and the regionality of communication between the tropics and the extratropics, and vice versa, as had been noticed in the diagnostic studies.

It was found that the sign and magnitude of a constant basic state altered the character of the modes considerably. In particular, the degree of trapping of the equatorial modes was altered. Waves were far less trapped in a westerly flow than in an easterly flow. In westerlies of order 10 m s^{-1} turning latitudes of equatorial modes may extend to 45° latitude compared with about 15° in an equivalent easterly (Fig. 10). Thus, one may expect that waves of similar scale would extend much further poleward in the upper troposphere of the eastern Pacific and Atlantic Oceans than elsewhere. Noting the variation of the mean state of the upper troposphere, shown in Fig. 2, it is expected that waves of similar scale would extend much further poleward in the upper troposphere of the eastern Pacific and Atlantic Oceans (in the vicinity of the westerly ducts) than elsewhere. Such behavior is in keeping with the observations of strong activity and interaction between the tropics and extratropics in these two regions.

Overall, the impact of latitudinal shear appears consistent with that found for the constant basic states. Where the shear is strongest and the equatorial flow is easterly, the modes are well trapped about the equator. On the other hand, where the shear is weak and the equatorial flow is westerly, the trapping is reduced. Thus, one may expect that equatorial transient events will effect the extratropics in the regions of the mid-Pacific and Atlantic trough regions.

It was also noted that the longitudinal shearing deformation in the tropics is about the same magnitude as in the middle latitudes. This feature of the tropical basic state was found to be extremely important in determining the nature of variance in the tropics. Horizontal stretching deformation in the tropics possesses the addition capability of causing wave energy accumulation. This is because there are zeros in the basic state. At high latitudes the horizontal stretching deformation is embedded in strong westerlies. Although a mode will be modified somewhat at higher latitudes (see Farrell and Watterson, 1985) it cannot achieve a zero Doppler-shifted group speed. On the other hand, in the tropics, because of the zeros in the basic state, over a wide range of modes, in particular the Rossby family and the westward propagating mixed Rossby-gravity mode, zeros in the Doppler shifted longitudinal group velocity component are possible. In fact, in a reasonable parameter range, a convergence of transient wave energy occurs in regions where $U_x < 0$ occurs. Accumulation into a particular region proceeds from the east ('forward' accumulation) for the long-wave packet, and, from the west ('backward' accumulation) for the short-wave packet which includes the mixed Rossby-gravity mode. Thus, for a wide range of scales, the westerlies of the upper troposphere of the Pacific and Atlantic Oceans act as 'attractors' of transient equatorial modes.

The phenomena of longitudinal energy accumulation accounts for why there may be regions of transient variance in specific regions of the tropics. Coupled with the impact of the sign and magnitude of the basic state, it can be understood why the accumulating modes extend or 'emanate' to higher latitudes and why the mid-ocean trough regions are so important in understanding the interaction of the tropics and middle latitudes.

It was also noted that there is a strong annual variation in the accumulation and emanation phenomena. The strongest accumulation corresponds, of course, to the times of the year when the equatorial stretching deformation is strongest. Thus, accumulation is a maximum in the eastern Pacific and the central Atlantic Oceans during the boreal winter (DJF) but almost non-existent during the summer (JJA). There is a strong interannual variability of accumulation depending on the magnitude and sign of the SOI (Southern Oscillation Index). During. La Niña times (SOI $\gg 0$) the maximum DJF accumulation takes place in the Pacific Ocean. However, during El Niño periods (SOI $\ll 0$) when the westerlies are much stronger in the Atlantic than in the Pacific, the region of maximum accumulation changes to the Atlantic.

Longitudinal stretching deformation in the tropical atmosphere is strongly coupled with vertical shear. Also, equatorial modes possess a finite vertical group speed. The effects of the vertical propagation of equatorial modes appears to be rather important. It was shown that regions of horizontal accumulation correspond to the regions of maximum vertical propagation. This suggestion was supported by the ray tracing through relatively complicated basic flows. The mid-ocean trough regions once again emerge as very important regions. Besides being regions where horizontal accumulation occurs for both long- and short-wave packets, the modes also become less trapped and extend to higher latitudes. The longitudinal variation of vertical shear is so configured as to constrain the modes in the troposphere until they reach the accumulation zone. There, with the change of the sign of the vertical shear, the modes rapidly expand upwards into the stratosphere.

4.3. Errors and error propagation

Observational studies have indicated that there are specific zones of transient activity in the tropical atmosphere and probably well defined corridors of interaction between the tropics and higher latitudes. The theory of equatorial waves, here extended to take into account complicated and realistic basic flows, tends to explain the various observed concentrations of eddy variance.

In the introduction it was noted that there was distinct regionality in the climate drift of the NMC model (Fig. 1). Clearly, these error centers correspond to the observed location of the long-term average variance in the real atmosphere. Furthermore, they correspond to the regions where theory suggests that there should be an energy accumulation and wave extension or emanation. However, as the climate drift of a model is calculated as a difference field, the regionality of error must result from the accumulation of errors within a particular region.

The model results suggest that there should be a strong temporal variation in the wave propagation and the energy accumulation in the tropics. Perhaps a simple test would be to see if the same temporal variability existed in the climate drift of the model. If it could be shown that error (for example, resulting from the poor parametrization of convection in the warm pool regions of the Pacific Ocean) did propagate in the same manner as the modified transients, then there are two immediate benefits. In the first place, it would suggest a strategy that would help find the source of the errors. Also, if the errors moving away from their source regions obeyed the rules of equatorial waves moving through complicated basic states it should be possible to anticipate when and where, and if, such errors would be maximized or minimized.

4.4. Consolidation

There are two major consolidations required of the work discussed in this paper.

4.4.1. Equatorial and extratropical waves

It was also noted that observational results of the penetration of extratropical waves into the deep tropics (Tomas and Webster, 1994) were consistent with the theoretical and modelling results of Webster and Holton (1982). Specifically, modes could advance deeply into the tropics and probably into the other hemisphere if no critical latitude existed such as in the vicinity of the westerly ducts. However, because of the vertical

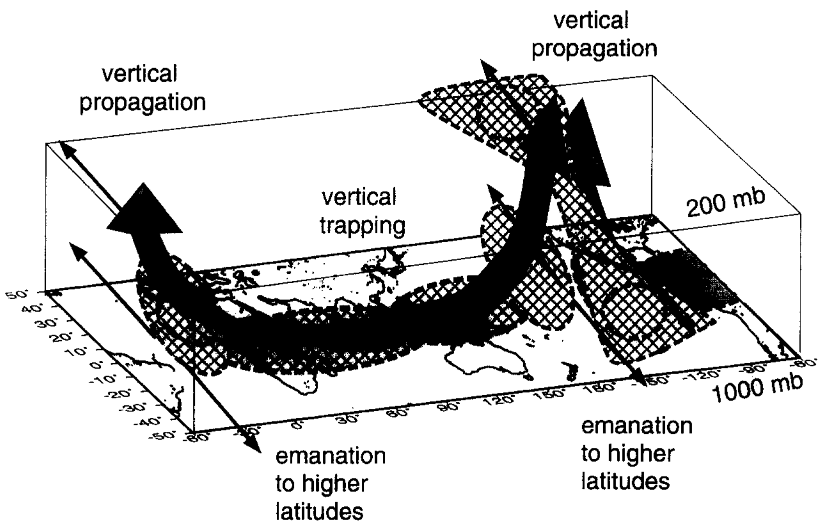

Fig. 20. Schematic diagram of wave propagation in and out of the westerly duct. The diagram shows the three-dimensional trajectories of waves forced in the convective regions of the tropics. Wave packets either move eastward or westwards depending on type and/or scale in to the regions of the westerly ducts. There they emanate to higher latitudes and to higher levels in the atmosphere.

shear and the existence of the easterly dome below the westerly duct, the equatorwardly propagating mode is forced to tilt in the vertical (Tomas and Webster, 1994). Similarly, equatorial modes tend to accumulate near the westerly duct in regions of negative stretching deformation either through forward or backward accumulation processes (Chang and Webster, 1995). At these locations the modes also extend poleward to higher latitudes. But the vertical shear also has an effect. The westerly ducts are also regions of positive vertical shear whereas the easterly regime possesses reverse shear. Thus, in the westerly ducts modes are freer to propagate vertically. Fig. 20 shows a schematic of transient characteristics.

4.4.2. A homogeneous approach

In order to ensure analytic tractability, the inhomogeneities of the basic flow were considered piecemeal and with different models. For example, horizontal shear and longitudinal stretching deformation were considered separately in a free surface barotropic model. Vertical shear and longitudinal stretching deformation were considered using a vertically dependent model but with local WKB approximations. Furthermore, to assure separability, only an isothermal atmosphere was considered. Thus, wave propagation through a fully three-dimensional basic state was not considered simultaneously. Whereas it is felt that the rudimentary constraints and modifications of basic state homogeneities were elucidated, there is still an element of uncertainty regarding their role if they were to act simultaneously. Finally, there is the question of the definition of a basic state. This question stems from the uncertainty of temporal scale separations between the wave and the variability of the basic state.

In order to tackle these two problems, it is necessary to use the next level of complexity of models. Work is currently under way with colleagues at the ECMWF using the operational model in experimental format. Experiments are being conducted where perturbations representing wave sources are followed through the model evolution relative to a control model run.

Acknowledgements

This work was initiated while PJW was on sabbatical at the European Centre for Medium Range Weather Forecasts. An earlier version of the paper appeared in Webster (1992) as a report for the ECMWF Seminar Series. We wish to thank ECMWF for the use of their facilities and Drs T.N. Palmer and A. Hollingsworth for many interesting discussions. We would also like to thank Prof. J.R. Holton and an anonymous reviewer for constructive comments. Thanks are due to Kamram Sahami for help with the graphics.

This work was conducted under sponsorship of the Climate Dynamics Division of the National Science Foundation through grant NSF 95-26030 and ECMWF.

Finally, this article is dedicated to Richard Pfeffer for his scientific leadership during the last few decades and for the insights he has provided regarding the general circulation. One of us (PJW) was fortunate enough to take a course on the atmospheric general circulation from Professor Pfeffer. It was an extraordinary course delivered with

an enthusiasm typical of Dick Pfeffer and provided a view of the planet that was well ahead of the time. Many of the ideas that have appeared in our later papers were probably spawned in that class.

Appendix A. Wave equation in stratified flow

Following Lindzen (1967), we rewrite Eqs. (11)–(15) using the following transformations and solutions:

$$\begin{Bmatrix} u \\ v \\ w \\ \rho \\ p \end{Bmatrix} = \begin{Bmatrix} \sqrt{\rho_0}\, u \\ \sqrt{\rho_0}\, v \\ \sqrt{\rho_0}\, w \\ \rho/\sqrt{\rho_0} \\ p/\sqrt{\rho_0} \end{Bmatrix} \sim \begin{Bmatrix} \hat{u}(y,z) \\ \hat{v}(y,z) \\ \hat{w}(y,z) \\ \hat{\rho}(y,z) \\ \hat{p}(y,z) \end{Bmatrix} e^{i(kx-\omega t)} \tag{A1}$$

Substituting Eq. (A1) into Eq. (11) and combine them into one equation in term of $\hat{v}$ gives a horizontal structure equation:

$$\left[\frac{d^2}{dy^2} - \frac{k}{\omega}\beta - \frac{k^2\beta^2}{\omega^2}y^2\right]\Psi_n = \left(\frac{1}{gh_n} - \frac{k^2}{\omega^2}\right)(\beta^2 y^2 - \omega^2)\Psi_n \tag{A2}$$

and a vertical structure equation:

$$\tilde{V}_{n_{zz}} + \left[\frac{N_s}{gh_n} - \frac{(1-\epsilon)^2}{4H^2} - \frac{1}{2}\frac{d\epsilon}{dz}\frac{1-\kappa}{H(\kappa-\epsilon)} + \frac{1}{2}\frac{d^2}{dz^2}\ln N_s - \left(\frac{1}{2}\frac{d}{dz}\ln N_s\right)^2\right]$$
$$\tilde{V}_n = 0 \tag{A3}$$

where it has been assumed that $\tilde{v}$ is separable into a vertical and horizontal part:

$$\tilde{v} = \sum V_n(z)\Psi_n(y) \tag{A4}$$

where $V_n(z)$ and $\Psi_n(y)$ represent vertical and latitudinal structures of $\hat{v}$ separately. Also, the transformation $\tilde{V}_n = V_n/\sqrt{N_s}$ has been used. h_n represents a separation constant, $H = RT(z)/g$ the scale height of the basic state, $\epsilon(z) = dH/dz$, $\kappa = (\gamma - 1)/\gamma$ and $N_s = g(\kappa - \epsilon)/H$. It is assumed, following Lindzen (1967), that the forcing can be expressed as:

$$\left(\frac{\partial}{\partial y} + \frac{k}{\omega}\beta y\right)\left(\frac{\partial}{\partial z} - \frac{1-\epsilon}{2H}\right)\left(\frac{\sqrt{\rho_0}\, J}{\kappa - \epsilon}\right) = (\beta^2 y^2 - \omega^2)\sum_n S_n(z)\Psi_n(y) \tag{A5}$$

where S_n represents the vertical structure function of the forcing J.

References

Arkin, P., Webster, P.J., 1985. Annual and interannual variability of the tropical–extratropical interactions: an empirical study. Mon. Weather Rev. 113, 1510–1523.

Bjerknes, J., 1969. Atmospheric teleconnections from the equatorial Pacific. Mon. Weather Rev. 97, 163–172.

Blackmon, M.L., Wallace, J.M., Lau, N.-C., Mullen, S.L., 1977. An observational study of the Northern Hemisphere wintertime circulation. J. Atmos. Sci. 34, 1040–1053.

Boyd, J.P., 1978a. The effects of latitudinal shear on equatorial waves. Part I: Theory and methods. J. Atmos. Sci. 35, 2236–2258.

Boyd, J.P., 1978b. The effects of latitudinal shear on equatorial waves. Part II: Application to the atmosphere. J. Atmos. Sci. 35, 2259–2267.

Bretherton, F.P., Garrett, C.J.R., 1968. Wavetrain in inhomogeneous moving media. Proc. R. Soc. Lond. A362, 529–554.

Chang, H.-R., Webster, P.J., 1990. Energy accumulation and emanation at low latitudes. Part II: Nonlinear response to strong episodic equatorial forcing. J. Atmos. Sci. 47, 2624–2644.

Chang, H.-R., Webster, P.J., 1995. Energy accumulation and emanation at low latitudes. Part III: Forward and backward accumulation. J. Atmos. Sci. 52, 2384–2403.

Charney, J.G., 1969. A further note on large-scale motions in the tropics. J. Atmos. Sci. 26, 182–185.

Chen, C.-S., Trenberth, K.E., 1988. Forced planetary waves in the northern hemisphere winter: wave coupled orographic and thermal forcing. J. Atmos. Sci. 45, 682–704.

Farrell, B., Watterson, I., 1985. Rossby waves in opposing currents. J. Atmos. Sci. 42, 1746–1756.

Frederiksen, J.S., Webster, P.J., 1988. Alternative theories of atmospheric teleconnections and low-frequency fluctuations. Rev. Geophys. 26, 459–494.

Gelaro, R., 1990. The structure and dynamics of tropical–midlatitude interactions. Ph.D. Thesis, The Pennsylvania State University, University Park, PA, 213 pp.

Gill, A.E., 1982. Atmosphere and Ocean Dynamics. Academic Press, 662 pp.

Held, I.M., 1983. Stationary and quasi-stationary eddies in the extratropical troposphere: theory. In: Hoskins, B.J., Pearce, P.R. (Eds.), Large Scale Dynamical Processes in the Atmosphere. Academic Press, New York, pp. 127–167.

Hoskins, B.J., Karoly, D.J., 1981. The steady linear response of a spherical atmosphere to thermal and orographic forcing. J. Atmos. Sci. 38, 1179–1196.

Jacqmin, D., Lindzen, R.S., 1985. The causation and sensitivity of the northern winter planetary waves. J. Atmos. Sci. 42, 724–745.

Kasahara, A., 1980. Effect of zonal flows on the free oscillations of a barotropic atmosphere. J. Atmos. Sci. 37, 917–929.

Krishnamurti, T.N., 1979. Compendium of Meteorology, Vol. 2, Part 4—Tropical Meteorology. Rep. 364, World Meteorological Organizations Geneva, Switzerland.

Lighthill, J., 1978. Waves in Fluids. Cambridge University Press, 504 pp.

Lindzen, R., 1967. Planetary waves on a beta-plane. Mon. Weather Rev. 95, 441–451.

Matsuno, T., 1966. Quasi-geostrophic motions in the equatorial area. J. Meteor. Soc. Jpn. 44, 25–42.

O'Lenic, E., Webster, P.J., Samel, A.N., 1985. The effects of initial uncertainty in tropical analyses upon five-day forecasts with NMC'S Global spectral Model. NMC Technical Note #311.

Palmer, T.N., Anderson, D.L.T., 1994. The prospects for seasonal forecasting – a review paper. Q.J.R. Meteorol. Soc. 120, 755–793.

Palmer, T.N., Webster, P.J., 1995. Towards a unified approach to climate and weather prediction. Global Clim. Change 1, 265–280.

Philander, S.G., 1990. El Niño, La Niña, and the Southern Oscillation. Academic Press, New York, 293 pp.

Prinn, R., Gunnold, D., Simmonds, P., Alyea, F., Boldi, R., Crawford, A., Fraser, P., Grutzler, D., Hartley, D., Rusen, R., Rasmussen, R., 1992. Global average concentration and trend for hydroxyl radicals deduced from ALE/GAGE trichloromethane (methyl chloroform) data for 1978–1990. J. Geophys. Res. 97, 2445–2461.

Reynolds, C.A., 1993. Regional sources of error growth in the National Meteorological Center's medium-range forecast model. Ph.D. Thesis, The Pennsylvania State University, 204 pp.

Reynolds, C.A., Webster, P.J., Kalnay, E., 1994. Random error growth in NMC's global forecasts. Mon. Weather Rev. 122, 1281–1305.
Sardeshmukh, P.D., Hoskins, B.J., 1988. The generation of global rotational flow by steady idealized tropical divergence. J. Atmos. Sci. 45, 1228–1251.
Simmons, A.J., Wallace, J.M., Branstator, G., 1983. Barotropic wave propagation and instability, and atmospheric teleconnection patterns. J. Atmos. Sci. 40, 1363–1392.
Tomas, R., Webster, P.J., 1994. Horizontal and vertical structure of cross-equatorial wave propagation. J. Atmos. Sci. 51, 1417–1430.
Tracton, S., Mo, K., Chen, W., Kalnay, E., Krister, R., White, G., 1989. Dynamical extended range forecasting (DERF) at the National Meteorological Center. Mon. Weather Rev. 117, 1604–1635.
Tsuda, T., Murayama, Y., Wiryosumarto, H., Harijono, S.W.B., Kato, S., 1994. Radiosonde observations of equatorial atmospheric dynamics over Indonesia: (I) Equatorial waves and diurnal tides. J. Geophys. Res. 99, 10491–10506.
Wallace, J.M., Kousky, V.E., 1968. Observational evidence of Kelvin wave in the tropical stratosphere. J. Atmos. Sci., 25, 900–907.
Webster, P.J., 1981. Mechanisms determining the atmospheric response to sea surface temperature anomalies. J. Atmos. Sci. 38, 554–571.
Webster, P.J., 1982. Seasonality in the local and remote response to sea surface temperature anomalies. J. Atmos. Sci. 39, 41–52.
Webster, P.J., 1992. Low frequency variability in the tropics and extratropics. In: European Centre for Medium Range Weather Forecasts Seminar Proceedings: Tropical–Extratropical Interactions, 10–14 December 1990. ECMWF, Reading, England, pp. 167–220.
Webster, P.J., 1995. The annual cycle and the predictability of the tropical coupled ocean–atmosphere system. Meteorol. Atmos. Phys. 56, 33–55.
Webster, P.J., Chang, H.-R., 1988. Equatorial energy accumulation and emanation regions: impact of a zonally varying basic state. J. Atmos. Sci. 45, 803–829.
Webster, P.J., Holton, J.R., 1982. Cross-equatorial response to middle latitude forcing in a zonally varying basic state. J. Atmos. Sci. 39, 722–733.
Webster, P.J., Yang, S., 1989. The three-dimensional structure of perturbation kinetic energy and its relationship to the structure of the wind field. J. Clim. 2, 1210–1222.
Whitham, G.B., 1965. A general approach to linear and nonlinear dispersive wave using a Lagrangian. J. Fluid Mech. 22, 273–283.
World Climate Research Programme (WCRP), 1985, International implementation plan for TOGA, ITPO Document #1, (first edition), W.M.O., Geneva.
Yanai, M., Maruyama, T., 1966. Stratospheric wave disturbances propagating over the equatorial Pacific. J. Met. Soc. Jpn. 44, 291–294.
Yang, S., Webster, P.J., 1990. The effect of summer tropical heating on the location and intensity of the extratropical westerly jet streams. J. Geophys. Rev. 95, 18705–18721.
Zhang, M., Geller, M.A., 1994. Selective excitation of tropical atmospheric waves in wave-CISK: the effect of vertical wind shear. J. Atmos. Sci. 51, 353–368.
Zhang, C., Webster, P.J., 1989. Effects of zonal flows on equatorially trapped waves. J. Atmos. Sci. 46, 3632–3652.